ENGINEERING RESEARCH INSTITUTE
THE UNIVERSITY OF MICHIGAN
ANN ARBOR

Final Report

THE GENERATION OF GUSTS IN A WIND TUNNEL AND MEASUREMENT OF UNSTEADY LIFT ON AN AIRFOIL

WADC Technical Report No. 57-401

L. C. Garby
A. M. Kuethe
J. D. Schetzer

Department of Aeronautical Engineering

Project 2099

DEPARTMENT OF THE AIR FORCE
WRIGHT AIR DEVELOPMENT CENTER
WRIGHT-PATTERSON AIR FORCE BASE, OHIO
CONTRACT NO. AF 33(616)316
PROJECT NO. 53-670A-686 AND 52-670A-86

June 1957

TABLE OF CONTENTS

LIST OF ILLUSTRATIONS

LIST OF ILLUSTRATIONS
(Concluded)

ABSTRACT

This report covers the work done under Contract No. AF 33(616)-316 between The University of Michigan and Wright Air Development Center of the United States Air Force. The work includes (1) the development of the equipment first on a small scale and measurements in a small wind tunnel; (2) the design and fabrication of a low-turbulence wind tunnel with a 5-foot x 7-foot working section [according to specifications developed in the low-speed work under (1)]; (3) construction of equipment for tests in the large tunnel; (4) tests of an airfoil at low and high angles of attack during passage through a gust; and (5) analysis of the results and comparison with theory where possible.

OBJECTIVE

The object of the work was to develop facilities for the measurement of gust loads and to demonstrate their feasibility at Reynolds numbers high enough to permit application of the results to full-scale flight.

INTRODUCTION

With increasing size, range, and complexity of aircraft, it is becoming important to determine more closely the effects of atmospheric gusts upon aircraft. Experimental information has been obtained largely in two ways: by full-scale flight tests through turbulent air, and from experimental model techniques in which the gust is simulated. Atmospheric turbulence is made up of a large number of gusts statistically distributed in intensity and scale. A particular cross section of the atmosphere through which an aircraft flies is repeatable, therefore, only in its statistical aspects. Flight-test work can, in general, only give a gross response, and will not easily yield details as to the exact manner in which the gust acts upon the aircraft. To provide the designer with more information, and to point the way for theoretical work, an experimental approach is needed.

UNSTEADY AERODYNAMIC EFFECTS

If the flow field about an aircraft is changing rapidly, certain nonstationary effects come into play that make the lift and moment on the aircraft depart from their "quasi-steady" values. The term "quasi-steady" is used to denote the time-varying force that, at any instant, is equal to the steady-state value corresponding to the flow configuration at that instant. The difference between the true dynamic lift and the quasi-steady value is called the lift lag.

The details of the various contributions to the lift lag are not understood for wing-body-tail combinations in which interference effects play a prominent role. For wings alone at subsonic speed, the lift lag is produced by the wake that accompanies the time-varying circulation and by the inertial reaction of the air to local acceleration. For simple plan forms, the so-called "wake lift" and "apparent-mass" lift can be predicted from the theory of thin airfoils. For a wing moving through a severe gust, the lift lag is known to be important. For a complete airplane with all interference effects considered, it is expected that the lift lag will also be a prominent factor. The lift lag is an essential feature of the gust problem and, therefore, gust-simulation equipment must include instrumentation that is adequate for measurement of the lift lag.

Tests on the pilot model of gust-simulation equipment which is described in the following sections have been run on a constrained two-dimensional wing. The theory for this case is well understood and has served as a guide for developing the instrumentation necessary to measure the lift.

Further tests in a 5-foot x 7-foot wind tunnel have verified the theory for two-dimensional flow and also indicate unsteady effects near maximum lift.

PREVIOUS WORK ON GUST SIMULATION AND RELATED PROBLEMS

Typical references to literature on problems related to the dynamics of aircraft flying through gusts are cited in this section. No attempt is made to give a complete bibliography on the subject.

It is believed that the only facilities presently in use for simulating the effect of atmospheric gusts are of the NACA Langley Field type (References 1 and 2), in which a model is flown through an updraft of controlled profile and the resulting motion is observed photographically.

Experiments in unsteady aerodynamics have been confined very largely to the measurement of forces and moments on models that are oscillated in a wind tunnel. The frequency information so obtained is used for arbitrary periodic motions by applying the superposition principle. Experiments of this type have been reported in the literature as early as 20 years ago, and they are currently being performed in ever-increasing numbers. Representative experiments on wings, bodies, and wing-body combinations are described in References 3 through 6.

Unsteady forces and moments have been calculated from the theory of thin air foils for two- and three-dimensional wings moving through an incompressible fluid, and also for wings moving subsonically and supersonically through a compressible fluid. Numerical data appear in the literature in the form of the indicial admittance (response to a unit step input) and the aerodynamic transfer function (response to a sinusoidal input). The response to an arbitrary input is found by Duhamel integration, using the indicial admittance, or Fourier synthesis, using the transfer function. Representative theory and calculations on nonstationary aerodynamics appear in References 7 through 16.

Among the earlier experiments on unsteady flow are those described in Reference 17, in which an airfoil was set in motion in a water tank and the flow pattern made visible by shining light on suspended oil globules. The circulation build-up during the first few chords of airfoil travel was calculated from the motion of the globules. Direct force measurements were obtained on a wing near the stall and rotated at a rate of one degree in 2.5 chords of wing travel (Reference 18). The circulation build-up on a wing was determined by taking hot-wire measurements of the flow pattern around the tip-trailing vortices as the wing passed through an updraft of known profile (Reference 19).

Calculations of the response of aircraft to gusts of given profile have appeared abundantly in the literature. A complete investigation requires that the rigid and elastic degrees of freedom of the aircraft be considered in investigating the response as the craft penetrates gusts of various sharpness. Though there is no difficulty in principle in assuming many degrees of freedom, the computational labor is great, and most investigators have considered only a small number. Typical examples of these calculations are given in Reference 20, in which the authors have calculated the response of a rigid airplane to gusts of various degrees of sharpness, considering the plunging degree of freedom only.

Calculations have been made using both steady- and unsteady-flow theory. In Reference 21, the response of an airplane entering a sinusoidal gust, with the

plunging and wing-bending degrees of freedom considered, has been calculated. Calculations on the influence of unsteady flow and structural flexibility on the rigid-body oscillations of an aircraft are numerous; typical examples are given in References 22 through 25. A general treatment of dynamics calculations is given in Reference 26. Finally, the nature of atmospheric turbulence, as deduced from meteorological measurements or the response of an airplane, is reported in the literature, and typical examples are given in References 27 through 31.

EXPERIMENTAL TECHNIQUES

To devise an experimental technique to check theoretical predictions and to provide design data, the following qualifications or criteria were established.

REPEATABILITY

The gust pattern and response must be repeatable under similar circumstances and these conditions must be capable of controlled variation.

GUST TESTING

The mechanism of the gust should be such that the model is either entering or emerging from the gust. It is in this transitional period that the lift lag occurs.

GUST STRUCTURE

The gust structure should preferably be a monotonic and rapid increase or decrease in angle of attack. A monotonic variation will in general be more reproducible, and the calculations necessary for a comparison with theory will be less involved than for more complicated gust structures. The more rapid the variation of angle of attack, the greater will be the lift lag, and hence greater accuracy will be obtainable in its measurement.

DYNAMIC VELOCITY

The mean velocity in the wind-stream direction should remain as constant as possible, making the gust effect one of an angle-of-attack change that can be reproduced in a quasi-steady manner.

QUASI-STEADY EFFECT

The mechanism producing the gust should be such that the gust pattern can be locked across the model. Quasi-steady measurements can then be made and the lift lag determined experimentally.

It was felt that along with the above conditions, and if at all possible, the model should be fixed in the tunnel and the gust passed over it, rather than the reverse. The instrumentation for the measurement of forces and for control of angle of attack is much simpler for a fixed than for a moving model.

The passage of a gust across a fixed model may be achieved in two ways: (1) a disturbance placed in the flow upstream of the model will be carried past the model by the tunnel flow; and (2) a continuous variation of the boundary conditions at the tunnel wall will cause an angle-of-attack change to sweep past the model.

Descriptions of the devices used for generating gusts are given below, followed by a detailed description of the experimental equipment and measurement technique.

For the first device, that of generating a disturbance and allowing the flow to carry the disturbance, the following system was used. A "Venetian blind" arrangement of airfoils (slats), referred to hereafter as a Vortex Gust Generator, was placed in the tunnel upstream of the model. A spring-loaded mechanism permitted a rapid change of angle of attack of the slats up to 10° and return to 0° in about 1/25 second. The vortex sheets shed by the slats during their motion were carried downstream and simulated a severe gust when they passed over the model. A schematic diagram is shown in Figures 1a and 1b.

The other technique was that of changing the wall boundary conditions. This is done by moving a bump along the floor of the tunnel. The flow field which passes over the model, shown schematically in Figure 2, simulates the emergence of the model from a gust, whose severity depends upon the rate of movement of the bump and the airspeed.

To carry out this program, two wind tunnels were used. Initial development of the Vortex and Moving Bump Gust Generator models was carried out in a small open-return tunnel having a nominal test-section dimension of 21 inches x 29 inches. A sketch of the tunnel with pertinent dimensions is given in Figure 3. Details of the configuration are given in Appendix I. A second tunnel was used to extend the results of the Moving Bump Gust Generator model by increasing the Reynolds number. A sketch of this tunnel is shown in Figures 4a and 4b, and details of its configuration are given in Appendix I.

Shown in Figure 5 are mechanical details of the Vortex Gust Generator. Figure 6 shows details of the Moving Bump Gust Generator for its installation in the first tunnel and its installation in the larger tunnel.

To measure the gust effect, the following measurements are made: position of bump in test section; angle of flow; and wind speed and normal force on wing model.

For the moving-bump tests, the position of the bump is measured by coupling the bump to a potentiometer. The bump position can be determined within an accuracy of ± 0.05 inch. Details of the system and circuit are given in Appendix II, part A. In Figure 7 are shown bump histories for a series of tests. It may be seen that the bump reaches its speed within approximately 1/2 chord and remains constant thereafter.

The angle of flow was measured for both the Vortex and the Moving Bump Gust

Generators by means of a hot-wire anemometer with a χ probe. An accuracy of ± 0.1 degree was limited by the accuracy of probe setting. A sensitivity of 0.02 degree was obtained by the electrical equipment. Methods of mounting and the circuitry are given in Appendix II, part B.

Typical angle-of-attack plots for the Vortex and Moving Bump Gust Generators are given in Figures 8 and 9.

Dynamic data were initially recorded on a dual beam DuMont oscilloscope with a Polaroid-Land camera that photographed the face of the scope. In the later tests, particularly those in the 5-foot x 7-foot tunnel, a Consolidated recording oscillograph was used.

The normal forces were measured by a single-component balance. The balance converted the normal force into either a rotational or translational displacement that was amplified and measured by means of a Schaevitz Linear Variable Differential Transformer. Details of the balance are given in Appendix II, part C.

Prior to and immediately after a series of dynamic runs, a quasi-steady run and calibration run were made to be certain that the data were consistent.

LIFT-LAG THEORY

A gust that sweeps across a wing causes a lift history that is different from the response that would occur if the gust pattern could be treated as a series of steady-state distributions across the wing. Part of this difference is caused by the fact that, as the lift changes, vorticity is shed from the trailing edge of the wing. These vortices are carried downstream by the flow and influence the normal velocity distribution across the wing chord. The other factor contributing to this difference is due to the force required to accelerate the air particles from one steady state to another. The various contributions are expressed by the equation:

$$L' = L_a + L_Q + L_W \quad . \tag{1}$$

Reference will continually be made to these components, whose symbols and definitions are given below.

Dynamic lift: L'. The complete lift experienced by the wing.
Quasi-steady lift: L_Q. The steady-state lift due to the normal velocity distribution of the gust.
Apparent mass lift: L_a. Lift acting on the wing due to the force required to accelerate the air particles from one steady state to another.
Wake lift: L_W. Lift on the wing due to a normal velocity distribution across the wing, imposed by vortices in the wake.
Lift lag: $L'-L_Q$. The difference between the dynamic and quasi-steady lift at any instant of time.

Reference 8 develops the dynamic lift in terms of the three components listed above. The equation is:

$$L' = -\rho \frac{\partial}{\partial t} \int_{-2b}^{2b} \gamma_Q \, X dX + \rho V_\infty \Gamma_Q + \rho V_\infty \int_{-2b}^{2b} \frac{\gamma(\xi)}{\sqrt{(\xi/2b)^2 - 1}} \, d\xi \quad , \qquad (2)$$

where

Γ_Q is the quasi-steady circulation,

γ_Q is the quasi-steady vorticity distribution across the wing, and

$\gamma(\xi)$ is the vorticity distribution in the wake.

The terms in the above equation are identified below:

$$L_a = -\rho \frac{\partial}{\partial t} \int_{-2b}^{2b} \gamma_Q \, X dX$$

$$L_Q = \rho \, V_\infty \Gamma_Q$$

$$L_W = \rho \, V_\infty \int_{-2b}^{2b} \frac{\gamma(\xi)}{\sqrt{(\xi/2b)^2 - 1}} \, d\xi$$

QUASI-STEADY AND APPARENT MASS LIFTS

Using the linearized theory for an airfoil of arbitrary camber distribution as given in Reference 34, the quasi-steady vorticity distribution γ_Q and circulation Γ_Q for a normal velocity distribution g(x) are:

$$\gamma_Q = \sum_{n=1}^{\infty} \frac{n \, B_n}{b^{n+1}} \left(\frac{1 - \cos n\theta}{\sin \theta} \right)$$

$$\Gamma_Q = 2\pi b \sum_{n=1}^{\infty} \frac{n \, B_n}{b^{n+1}}$$

$$\frac{n \, B_n}{b^{n+1}} = \frac{2}{\pi} \int_{-\pi}^{\pi} g(x) \sin n\theta \sin \theta d\theta$$

$$X = 2b \cos \theta$$

g(x) is the normal velocity distribution of the gust (see Figure 10). L_Q is solved for directly upon knowing the g(x) distribution. γ_Q can also be solved directly; the differentiation with respect to time is related to the speed at which the gust is passing over the wing.

The vorticity distribution in the wake is related to the quasi-steady circulation by the Helmholtz theorem, and the equation is:

$$\Gamma_Q(t) + \int_{2b}^{2b+V_\infty t} \left(- \frac{\xi/2b + 1}{\xi/2b - 1} \right)^{1/2} \gamma(\xi) d\xi = 0 . \qquad (3)$$

Thus $\gamma(\xi)$ may be obtained for any function of Γ_Q with time. The wake lift resulting from a unit step in Γ_Q (Wagner problem) has been computed (see Reference 8), and may be written as:

$$L_w(\sigma) = - \rho V_\infty \Phi(\sigma) . \qquad (4)$$

The function $\Phi(\sigma)$ can be approximated by:

$$\Phi(\sigma) = 0.165e^{-0.0455\sigma} + 0.355e^{-0.300\sigma} \qquad \text{(see Reference 9)} .$$

For an arbitrary Γ_Q distribution with time, the wake lift is found by using the superposition principle.

The equations given above are based upon the following assumptions:

1) Flow is two-dimensional.
2) Thin airfoil theory can be applied.
3) The wake remains flat.
4) The gust effect is that of a change of angle of attack across the airfoil.

It should be noted that all three terms on the right-hand side of Equation 2 are determined from quasi-steady values. These values are fixed by the normal velocity distribution across the wing.

TEST RESULTS

MOVING BUMP GUST GENERATOR

The first of the moving-bump tests were conducted in the small open-return tunnel described in Appendix I. The lift-sensitive wing had a chord of 6 inches and a span of 12 inches; two-dimensional flow was maintained by use of end plates. The angle-of-attack distribution for the gust passing over the wing is shown in Figure 8. This distribution passes over the wing at the speed with which the bump is moved. Figure 7 shows that the bump is rapidly accelerated to a constant speed.

As the bump moves with a velocity V_B, the normal velocity distribution as determined by quasi-steady measurements requires correction because the motion of the bump causes the streamlines to distort relative to the quasi-steady flow conditions (see Figure 11). The dynamic streamlines are flatter, and therefore the gust would be less intense than indicated by quasi-steady tests.

Typical lift responses for dynamic and quasi-steady runs are shown in Figure 12. It is seen that the effect indicated in Figure 11 is not discernible for the bump speed used. The experimental lift lag and theoretical lift lag are compared in Figure 13. It should be noted that the experimental and theoretical lift lags agree well up to their maximum values. However, the experimental results fall off faster than those computed by theory. No explanation is apparent at this time for this lack of agreement.

The maximum Reynolds number tested with the small tunnel was 148,000. A larger version that was identical in the gust mechanism was built to extend the Reynolds number. The tunnel and equipment are described in Appendix I. In Figure 7 the bump velocity is shown as a function of displacement and time. From this curve it can be seen that the bump has reached nearly uniform speed within the first 1/2 chord of travel (12-inch chord). The gust input, expressed as angle of attack, is shown as a function of bump position in Figure 8. These data include both quasi-steady and dynamic runs. There is no correction necessary for the effect of the bump motion upon the streamlines, but it was necessary to make a correction to the dynamic position of the bump because of the stretch of the position-indicator cable.

Tests were conducted at tunnel speeds of 72.5, 55, and 20 feet per second. Bump speeds of 14.3, 12.5, and 10.1 feet per second were used. At lower speeds a superimposed oscillation was picked up by the wing. The fluctuation of this oscillation was such that the results were not conclusive. Due to insufficient time and money, only the results of the test at the speed of 72.5 feet per second are analyzed and presented herein.

In Figure 14 are shown the quasi-steady and dynamic force responses as a function of time for a Reynolds number of 465,000. From these data the theoretical lift lag is computed and the experimental lift lag obtained, as shown in Figure 15. It should be noted that the experimental and theoretical lift lag are very similar to those measured in the 21-inch x 29-inch tunnel.

After completion of lift-lag tests, tests were made of lift overshoot at stall. The wing was set at a negative angle of attack sufficiently large to cause the wing to stall when the bump flow field was removed by moving the bump downstream (see Figure 16). The lift response is shown in Figure 17 for two bump speeds.

In Figure 18, the ratio of $C_{N\text{-Max}}$ (Dynamic Test) / $C_{N\text{-Max}}$ (Static Test) is plotted as a function of rate of change of angle of attack with time. The data definitely show that there is a measurable lift overshoot and that the technique used is capable of measuring flow details of the phenomena. The data of Figure 18 indicate that the ratio $C_{N\text{-Max}}$ (Dynamic Test) / $C_{N\text{-Max}}$ (Static Test) plotted against $d\alpha/dt$ gives a simple straight-line curve, within the limits of the tests.

The data given in Figure 18 demonstrate that loads of the order of 35 percent greater than the steady-state values can be reached when an aircraft enters a severe

gust at a high angle of attack. These results are preliminary, but they demonstrate a field of application of the gust-generating equipment. Two- and three-dimensional wings should be studied in detail to determine design criteria for flight through rough air at high angles of attack.

VORTEX GUST GENERATOR

Because there is no way of making the flow pattern stand still with the vortex generator gust-simulating device, quasi-steady values of the lift cannot be obtained. As described in References 32 and 33, the flow pattern and dynamic lift are measured simultaneously for each run. This makes repeatability unnecessary.

Tests were made at wind speeds of 15, 30, and 60 feet per second. Shown in Figure 19 are representative oscillograms for the above tunnel-speed conditions. In Figures 20a, 20b, and 20c are shown the reduced data for these tunnel speeds.

In Figure 20a are shown six runs at a tunnel speed of 59.7 feet per second. The variations in lift measurements follow the variations in flow as shown by the monitor wire.

The hot-wire probe is located 2-1/2 inches ahead of the leading edge of the airfoil. Velocity measurements made at this station indicate that the same velocity occurs there as occurs at the reference Pitot-tube point for the tunnel. Thus, for a tunnel velocity of 59.7 feet per second, 0.0035 second is required for the flow pattern to travel from the probe to the leading edge of the lifting surface. Similarly, it requires 0.0119 second for the pattern to travel from the probe to the trailing edge of the lifting surface. Referring to Figure 20a, it is observed that zero inclination of the stream occurs at 0.015 second while the lift crosses the zero axis at 0.042 second, giving a time lag of 0.027 second. With reference to the mid-chord of the airfoil, the time delay is $(0.0035 + 0.0119)/2 = 0.0077$ second. The difference between the measured time lag of 0.042 second and the time delay of 0.0077 second is attributable to the aerodynamic lift lag.

The maximum dynamic lift calculated from theory is about twice the experimental value shown in Figure 20a. Whether the theory is incorrect for velocity gradients of the magnitude indicated here, or the instrumentation is inadequate, is uncertain.

CONCLUSIONS

The feasibility of generating reproducible gusts of sufficient intensity and scale at Reynolds numbers high enough to permit the extrapolations of measured unsteady lift increments to full scale has been demonstrated. In a wind tunnel of low turbulence, reasonable accuracy in the determination of lift lag is demonstrated on an airfoil of 1-foot chord at a Reynolds number of 450,000. No difficulties are anticipated in increasing the Reynolds number to several times this value.

The "lift overshoot" at angles of attack above the steady-state stall was meas-

ured for two gust intensities. The maximum lift coefficient attained a value 35 percent above the steady-state value before stalling. A detailed investigation of this phenomenon represents an important potential use of the facility.

REFERENCES

1. Donely, P., An Experimental Investigation of the Normal Acceleration of an Airplane Model in a Gust, NACA TN 706, 1939.

2. Donely, P., Summary of Information Relating to Gust Loads on Airplanes, NACA TN 1976, 1949.

3. Bratt, J. B., and Scruton, C., Measurements of Pitching Moment Derivatives for an Airfoil Oscillating About the Half Chord Axis, Br ARC RAM, 1921.

4. Ashley, Zertarian, and Neilson, Investigation of Certain Unsteady Aerodynamic Effects in Longitudinal Dynamic Stability, MSAF TR 5986.

5. Buchan, Harris, and Summervail, Measurements of $Z_{\dot{w}}$ for an Oscillating Airfoil, College of Aeronautics, Cranfield Report No. 40.

6. Halfman, R. L., Experimental Aerodynamic Derivatives of a Sinusoidally Oscillating Airfoil in Two-Dimensional Flow, NACA TN 2465, 1951.

7. Theodorsen, T., General Theory of Aerodynamic Instability and the Mechanism of Flutter, NACA TR 496, 1935.

8. v. Kármán, Th., and Sears, W. R., "Airfoil Theory for Non-Uniform Motion," J. Aero. Sci., 5, 379-390, 1938.

9. Jones, R. T., The Unsteady Lift of a Finite Wing, NACA TR 681, 1940.

10. Luke, Y. L., Table of Coefficients for Compressible Flutter Calculations, USAF TR 6800.

11. Mazelsky, B., Determination of Indicial Lift and Moment of a Two-Dimensional Pitching Airfoil at Subsonic Mach Numbers from Oscillating Coefficients with Numerical Calculations for M = 0.7, NACA TN 2613, 1952.

12. Biot, M. A., "Loads on a Supersonic Wing Striking a Sharp Edged Gust," J. Aero. Sci., 16, 296-300, 1949.

13. Garrick, I. E., and Rubinow, S. I., Theoretical Study of Air Forces on an Oscillating or Steady Thin Wing in a Supersonic Main Stream, NACA TN 1383, 1947.

14. Reissner, E., Effect of Finite Span on the Airload Distribution for Oscillating Wings, NACA TN 1194, 1947; TN 1195, 1947 (with Stevens, J. E.).

15. Biot and Boehnlein, Aerodynamic Theory of Oscillating Wings of Finite Span, Calcit Report No. 5.

16. Wasserman, S., Aspect Ratio Corrections in Flutter Calculations, USAF MR MCREXA 5-4595-8-5.

17. Walker, P. B., Growth of Circulation About a Wing and Apparatus for Measuring Fluid Motion, Br ARC R and M 1402, 1931.

18. Farren, W. S., Reaction on a Wing Whose Angle of Incidence is Changing Rapidly, Br ARC R and M 1648, 1935.

19. Kuethe, A. M., Circulation Measurements About the Tip of an Airfoil During Flight Through a Gust, NACA TN 685, 1939.

20. Bisplinghoff, R. L., Isakson, G., and O'Brien, T. F., "Gust Loads on a Rigid Airplane with Pitching Neglected," J. Aero. Sci., 18, 33-42, 1951.

21. Kordes, E. E., and Houbolt, J. C., Evaluation of Gust Response Characteristics of Some Existing Aircraft with Wing Bending Flexibility Included, NACA TN 2897, 1953.

22. Goland, M., et al., Effects of Airplane Elasticity and Unsteady Flow on Longitudinal Stability, Midwest Research Institute Project No. R108E-108.

23. Statler, I. C., "Dynamic Stability at High Speed from Unsteady Flow Theory," J. Aero Sci., 17, 232-242, 1950.

24. Lyon, H. M., and Ripley, J., A General Survey of the Effects of Flexibility of the Fuselage, Tail Unit, and Control Systems on Longitudinal Stability and Control, Br ARC R and M 2415, 1950.

25. Pai, S. I., and Sears, W. R., "Some Aeroelastic Properties of Swept Wings," J. Aero. Sci., 16, 105-115, 1949.

26. Schetzer, J. D., Dynamics for Aerodynamicists, Douglas Aircraft Company, S M 14077, 1951.

27. Donely, P., Effective Gust Structure at Low Altitude as Determined from the Reactions of an Airplane, NACA TR 692, 1940.

28. Clementson, G., An Investigation of the Power Spectral Density of Atmospheric Turbulence, MIT Thesis, 1950.

29. Sherlock, R. H., Storm Loading and Strength of Wood Pole Lines and Study of Wind Gusts, Edison Electric Institute, 1936.

30. Br RAE Report, Aero 2341. High Altitude Gust Investigation.

31. Huss and Portman. Study of Natural Winds and Computation of the Austausch Turbulence Constant, Guggenheim Airship Institute, Report No. 149.

32. Kuethe, A. M., Schetzer, J. D., and Garby, L. C., Research Design Problems Relating to Facilities for Simulating the Aerodynamic Effects of Atmospheric Gusts on Aircraft Components, The University of Michigan, Engineering Research Institute Project 2099, Progress Report No. 4, 1953.

33. Kuethe, A. M., Schetzer, J. D., and Garby, L. C., Research Design Problems Relating to Facilities for Simulating the Aerodynamic Effects of Atmospheric Gusts on Aircraft Components, The University of Michigan, Engineering Research Institute Project 2099, Progress Report No. 5, 1954.

34. v. Kármán, Th., and Burgers, J. M., "General Aerodynamic Theory of Perfect Fluids," Aerodynamic Theory, ed. W. O. Durand, Vol. II, Calif. Inst. Tech., Pasadena, 1943.

APPENDIX I

DESCRIPTION OF TEST TUNNELS

A. OPEN-RETURN TUNNEL

Initial test work for both the Vortex and Moving Bump Gust Generators was done in a small open-return tunnel. A sketch of the tunnel is shown in Figure 3. Data pertinent to this tunnel are listed below.

Speed range: 0 - 65 feet per second
Turbulence level: 0.03 percent (at) V = 50 feet per second
Contraction ratio: 16
Nominal test section size: 21 inches high
29 inches wide
100 inches long

The tunnel was constructed so that test sections are interchangeable. One test section contained the Vortex Gust Generator, and another contained a Moving Bump Gust Generator.

Tunnel speed was controlled by changing the revolutions per minute of a fixed pitch fan. A Reeves Vari-speed drive is the mechanism of speed change.

B. CLOSED RETURN: 5-FOOT x 7-FOOT TUNNEL

Work was continued with the Moving Bump Gust Generator on a larger scale. For this, a tunnel was constructed as a joint effort between the Air Force and the University. Previous experience had indicated the importance of keeping the turbulence level as low as possible. Figure 4 shows the plan view and dimensions at critical stations.

Data pertinent to this tunnel are:

Speed range: 0 - 250 feet per second
Turbulence level: 0.02 percent (at) V = 100 feet per second
0.035 percent (at) V = 200 feet per second
Contraction ratio: 15
Test section size: 5 feet high
7 feet wide
25 feet long
Power plant: Ward-Leonard drive, 1250 horsepower available, 300 horsepower required at maximum condition
Fan: Fixed pitch, 10 blades of laminated wood
Maximum diffuser angle: 5.5 degrees except in rapid expansion section
Settling chamber: 5 screens, 30-mesh wire of 0.075-inch diameter spaced 30 inches apart. After the last screen there is a distance of 10 feet before the nozzle starts.

An artist's sketch of the tunnel is shown in Figure 4b. Rails for the moving bump to travel on are covered by the bottom corner fillets when gust tests are not being made.

APPENDIX II

INSTRUMENTATION DETAILS

A. BUMP-POSITION INDICATOR

To indicate the position of the bump in the test section for both dynamic and quasi-steady tests, a system as shown in Figure 6a was used. A cable attached to the nose of the bump is wrapped around the drum of a 10-turn potentiometer. Travel of the bump rotates the potentiometer. The electrical circuit used is shown in Figure 21.

To position the bump for quasi-steady measurements, holes were drilled through the floor of the test section at given distances downstream. A tight pin inserted through the hole would allow the bump to rest at a known position. These holes were located within ± 0.05 inch.

B. ANGLE-OF-ATTACK MEASUREMENTS

Angle-of-attack measurements were made using a hot-wire anemometer with a χ probe. The circuit used is shown in Figure 22. This arrangement was necessary because steady-state angles of attack are necessary for the flow measurement. At a given tunnel speed the hot wire is calibrated by rotating it through known angles. Tests are then conducted at the same tunnel speed and wire-heating currents.

C. SPEED MEASUREMENTS

A check was made of the influence of the bump upon the local wind speed in the vicinity of the wing trailing edge. With the bump in a forward position there is a slight speed increase. This falls off rapidly as the bump is moved back. A comparison made between the quasi-steady and dynamic speed effect shows no measurable difference. The measurement was made by using a hot wire mounted in the horizontal plane. A direct-current amplifier was used to amplify the effect of steady-state velocity changes.

D. BALANCE SYSTEM

The balance arrangements used operated on similar principles, those of carrying the lift load into a flexure beam and measuring its deflection by means of a Schaevitz Transformer. Two-dimensional flow was maintained for the Vortex Gust Generator balance by using wing stubs that extended from the ends of the lift-sensitive wing to the floor and ceiling of the tunnel. These stubs were not in direct contact with the lift-sensitive wing, but the gap was kept very small. For the moving-bump system, end plates were used to keep the flow two-dimensional. Figure 23a shows details of a balance system for the Moving Bump Gust Generator. The arrangement of the stiff flexure beams was such that the model was sensitive only to the normal force.

To give a good dynamic response, the frequency of the wing-balance combination was kept as high as possible. The frequency response was checked by using a mechanical shaker and, for a given force input, measuring the balance output. The frequency response was found to be flat out to 40 cycles. A Fourier analysis of the gust function indicated that components beyond 10 cycles per second are negligible.

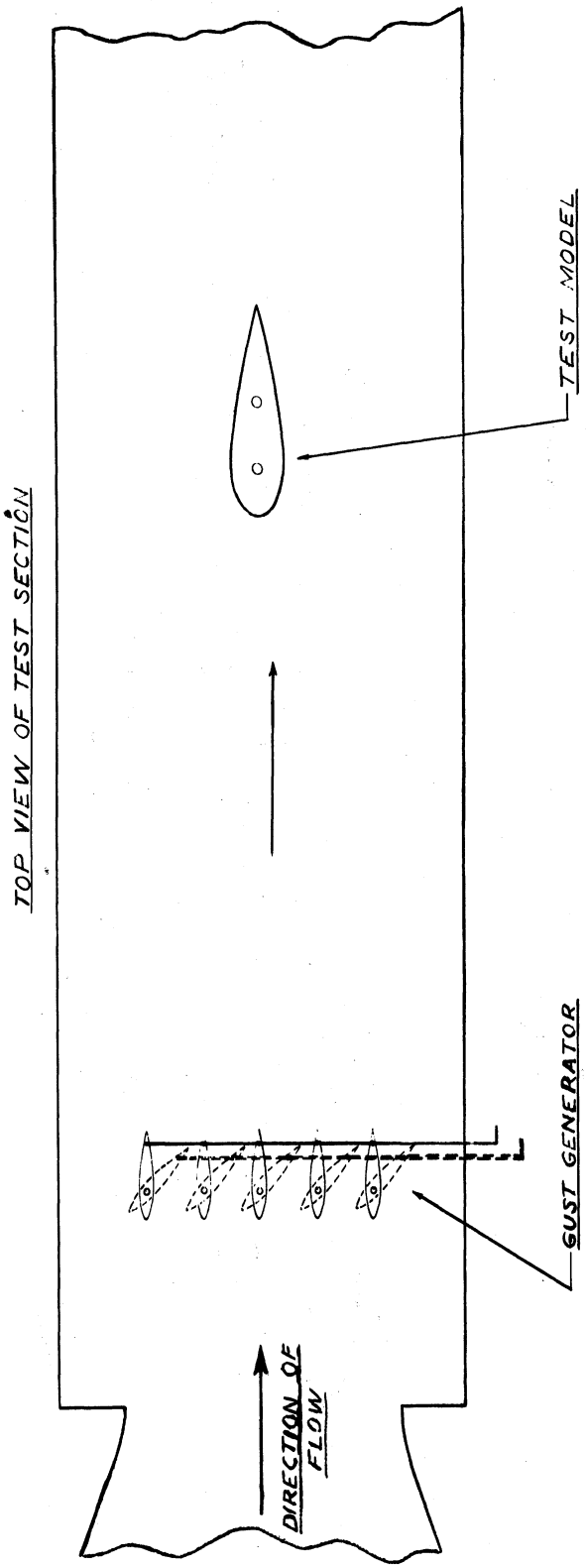

Figure 1a. Schematic diagram of Vortex Gust Generator.

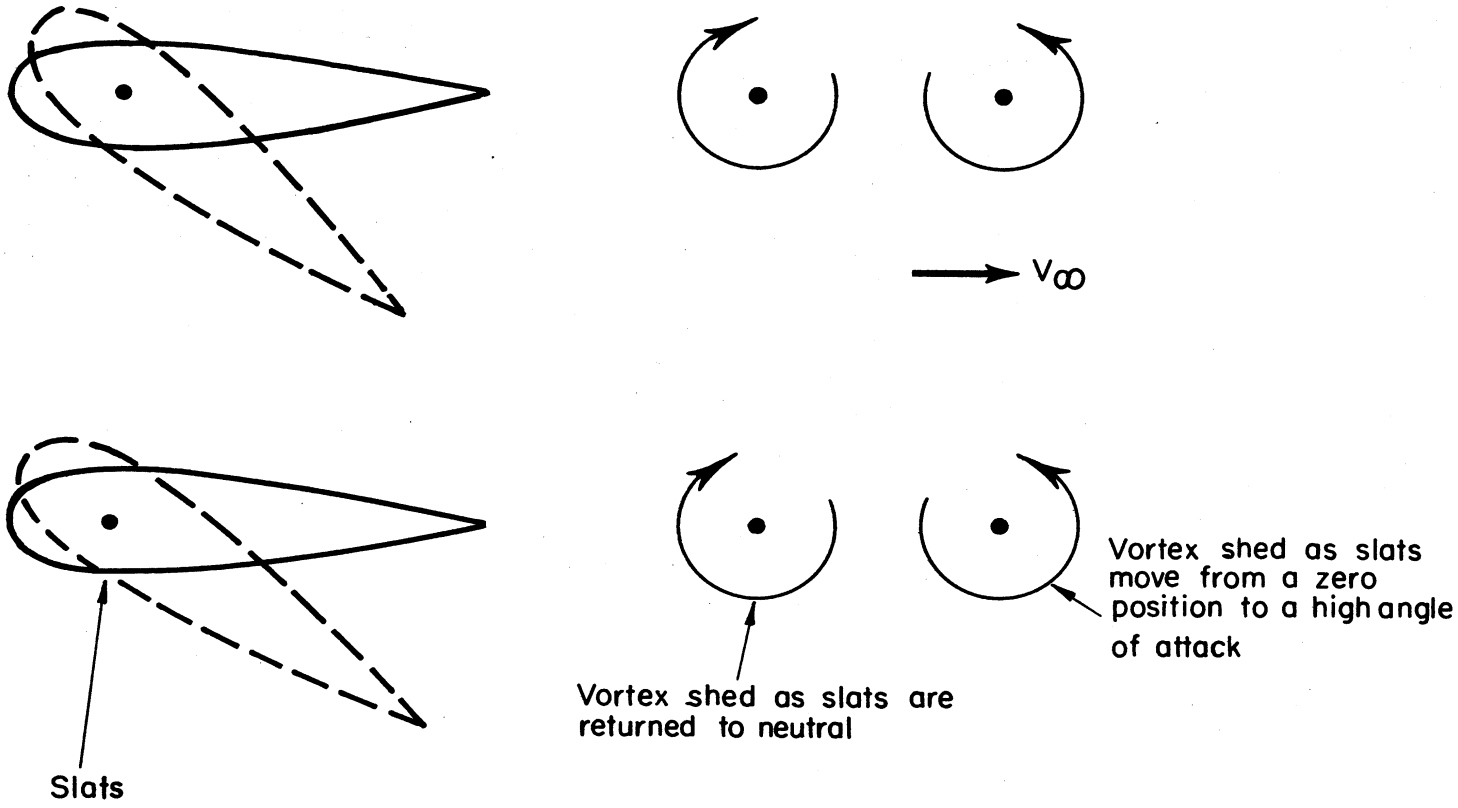

Figure 1b. Sketch showing vortex pattern formed by action of the slats.

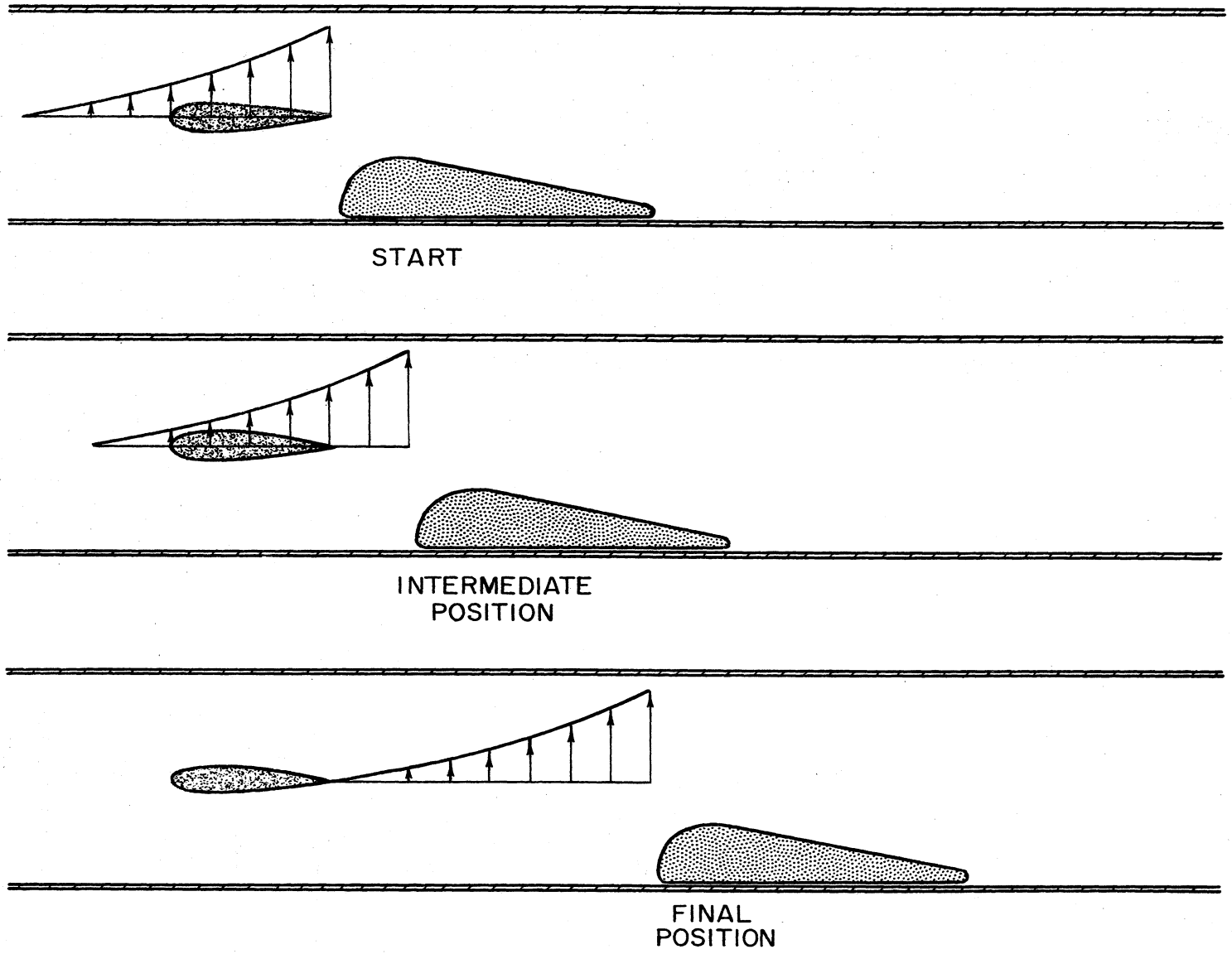

Figure 2. Normal velocity distribution for three positions of the bump.

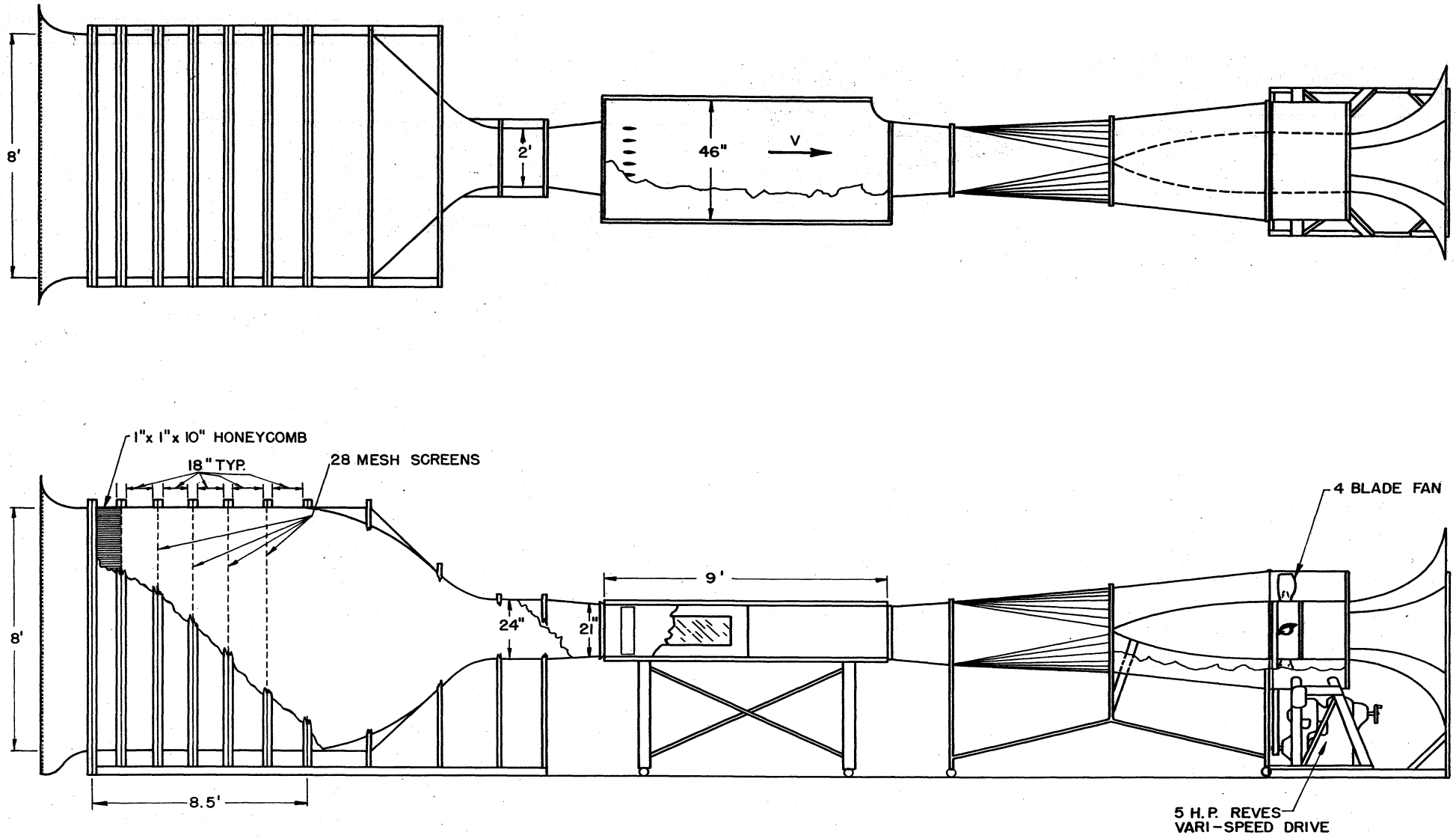

Figure 3. Open-return tunnel. The Vortex Gust Generator is shown. The Moving Bump Gust Generator is built into another test section that is interchangeable with the above.

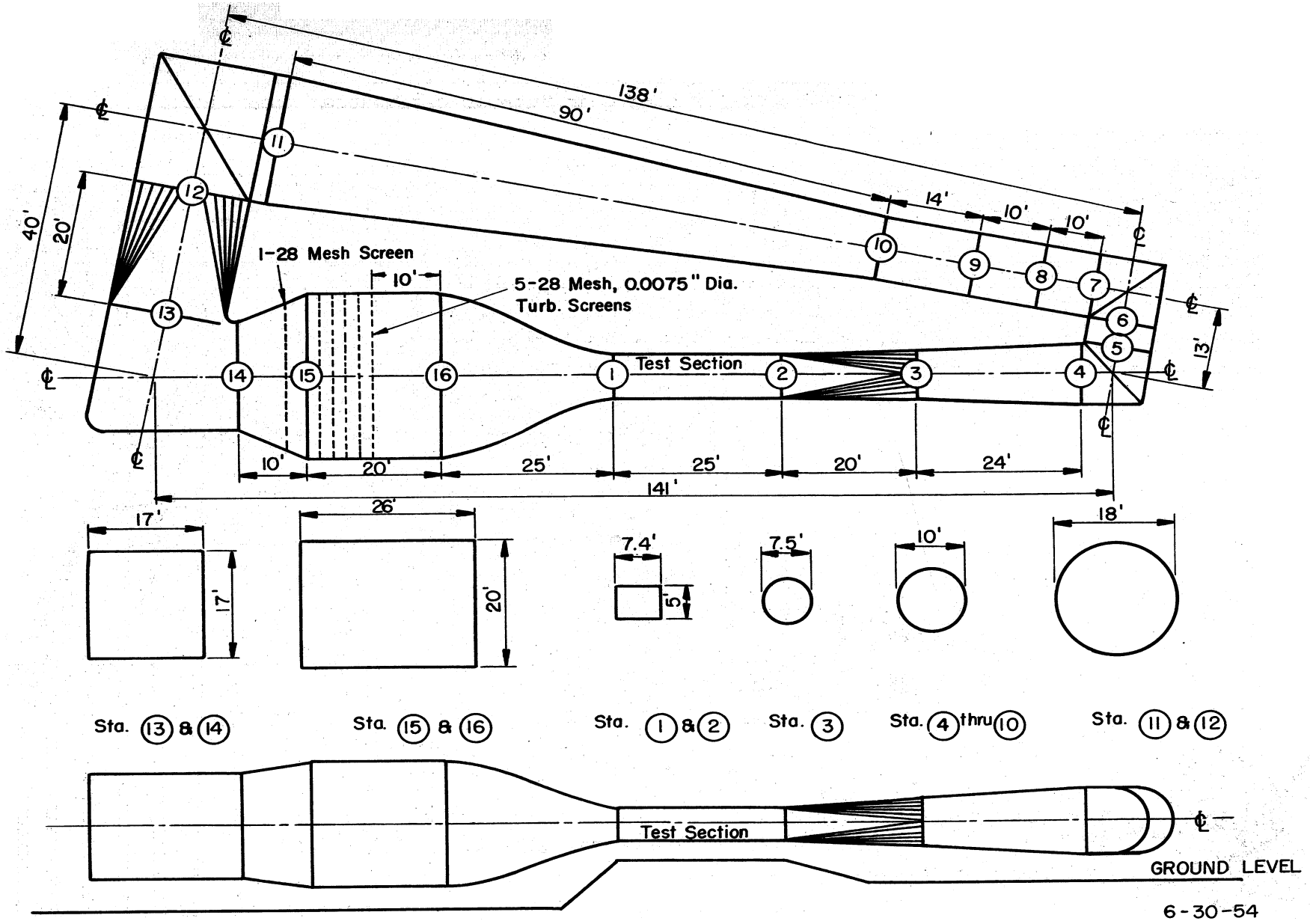

Figure 4a. Plan view of 5-foot x 7-foot gust-generator model.

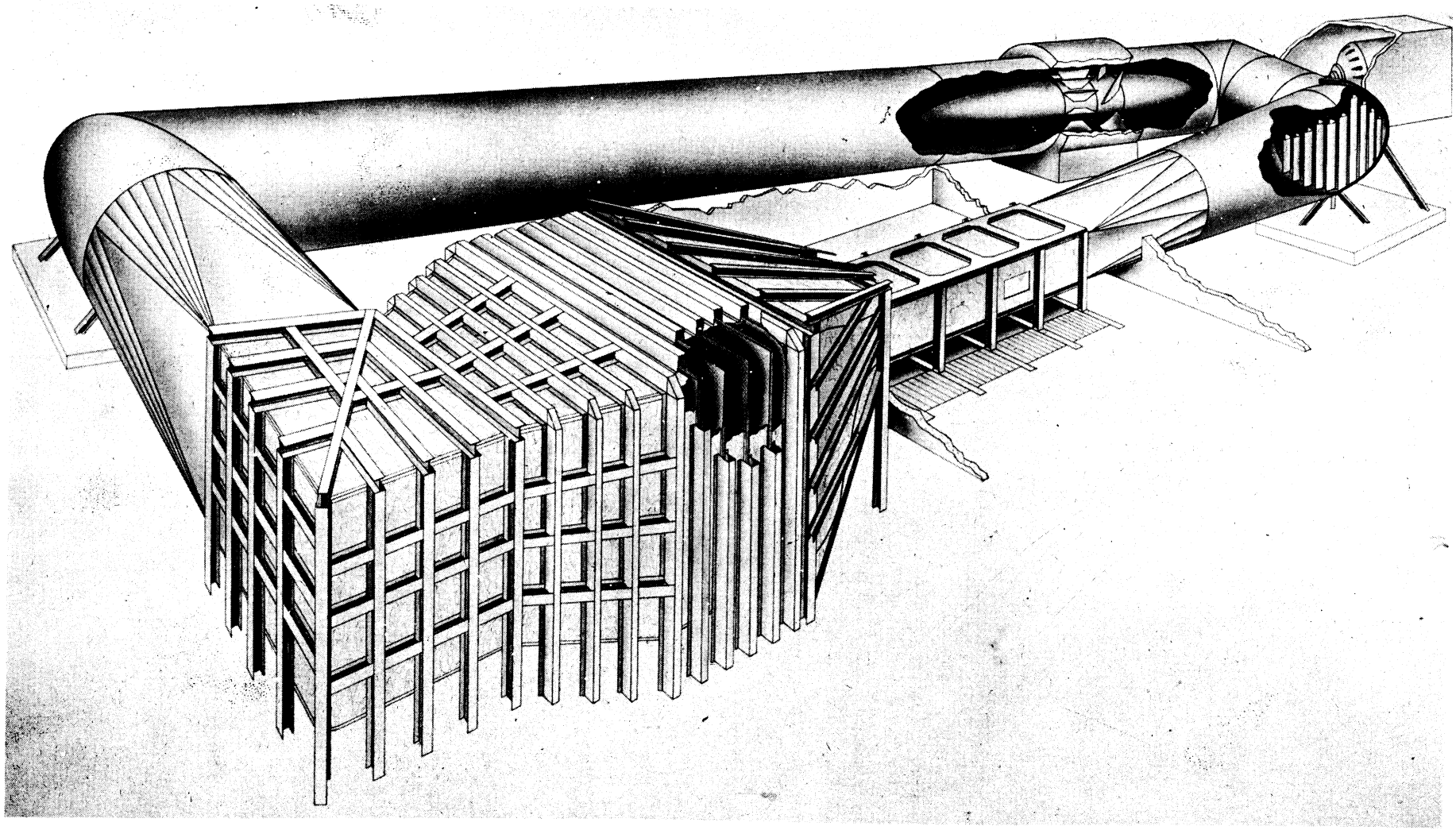

Figure 4b. Perspective drawing of 5-foot x 7-foot gust-generator model.

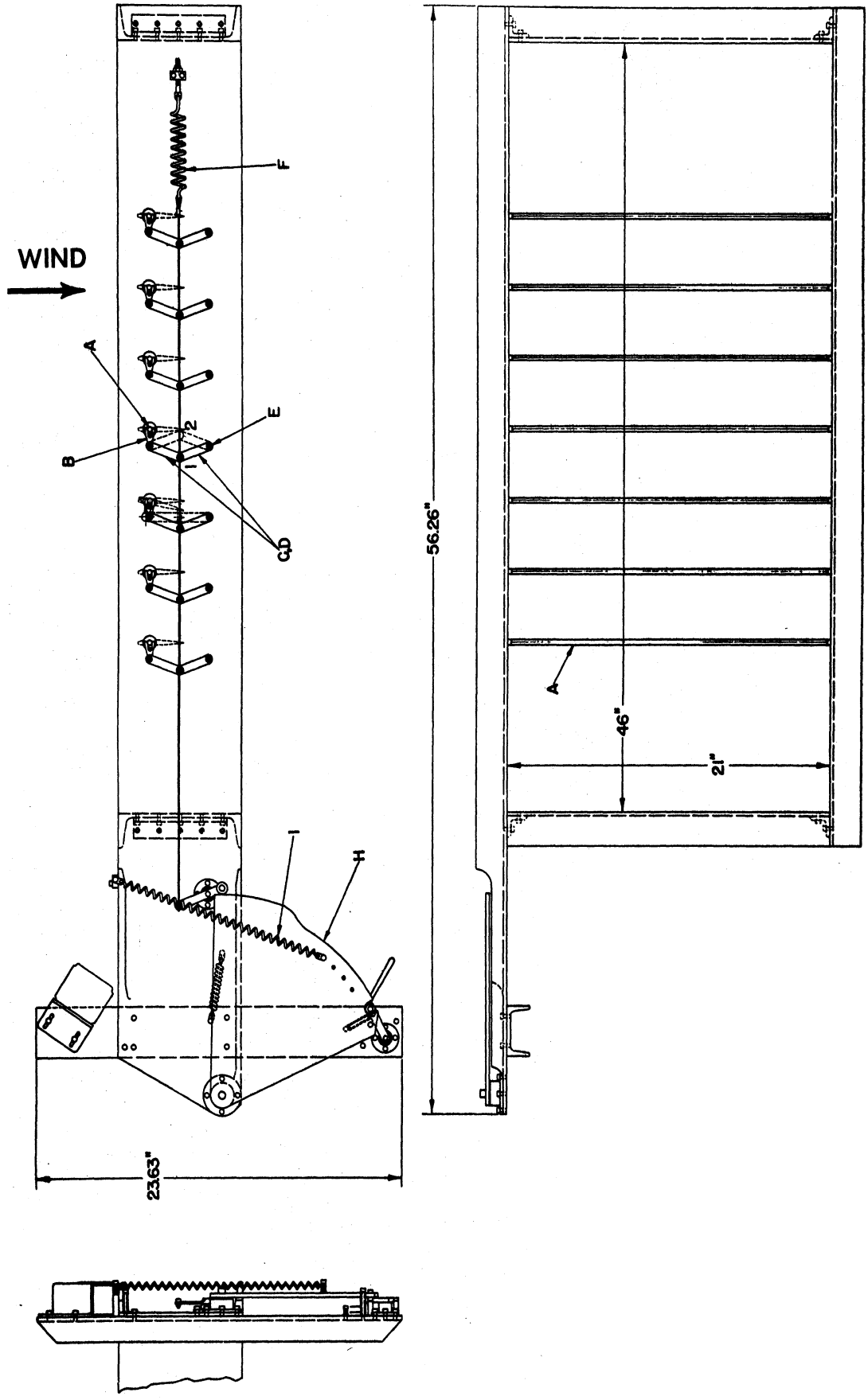

Figure 5a. Schematic drawing of Vortex Gust Generator mechanism.

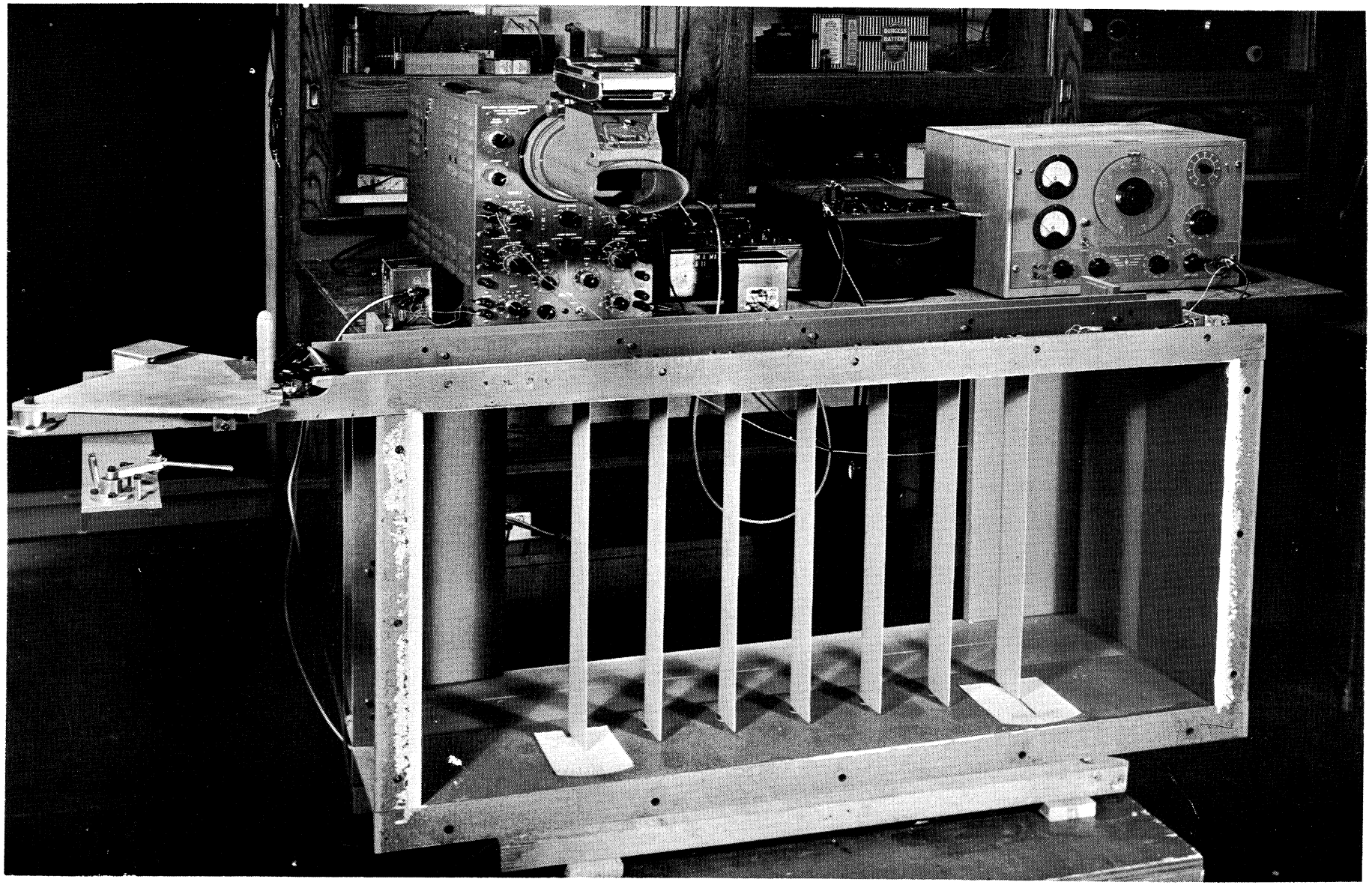

Figure 5b. Photograph showing bench calibration of Vortex Gust Generator and the associated electrical equipment.

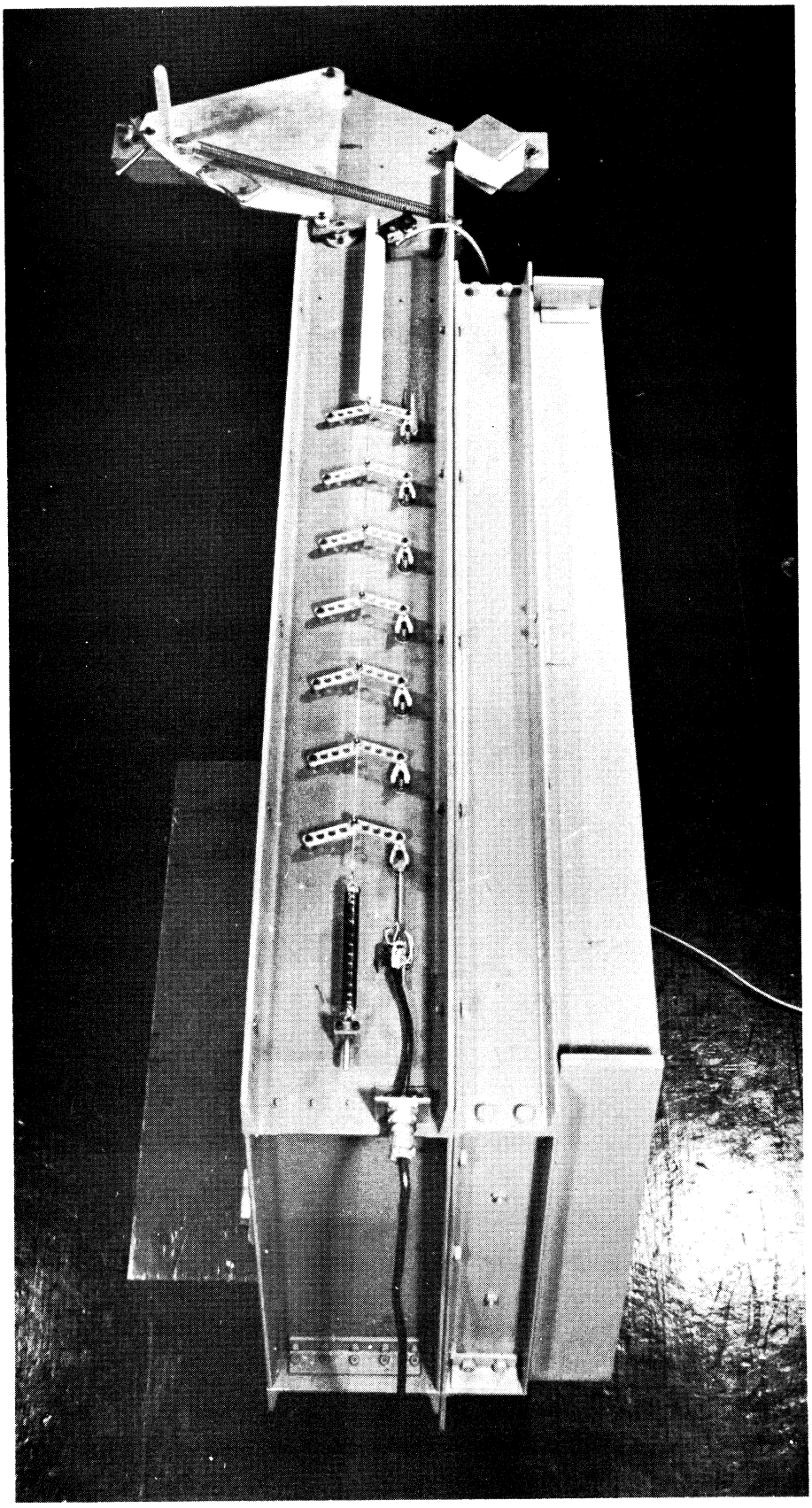

Figure 5c. View of linkage mechanism of Vortex Gust Generator.

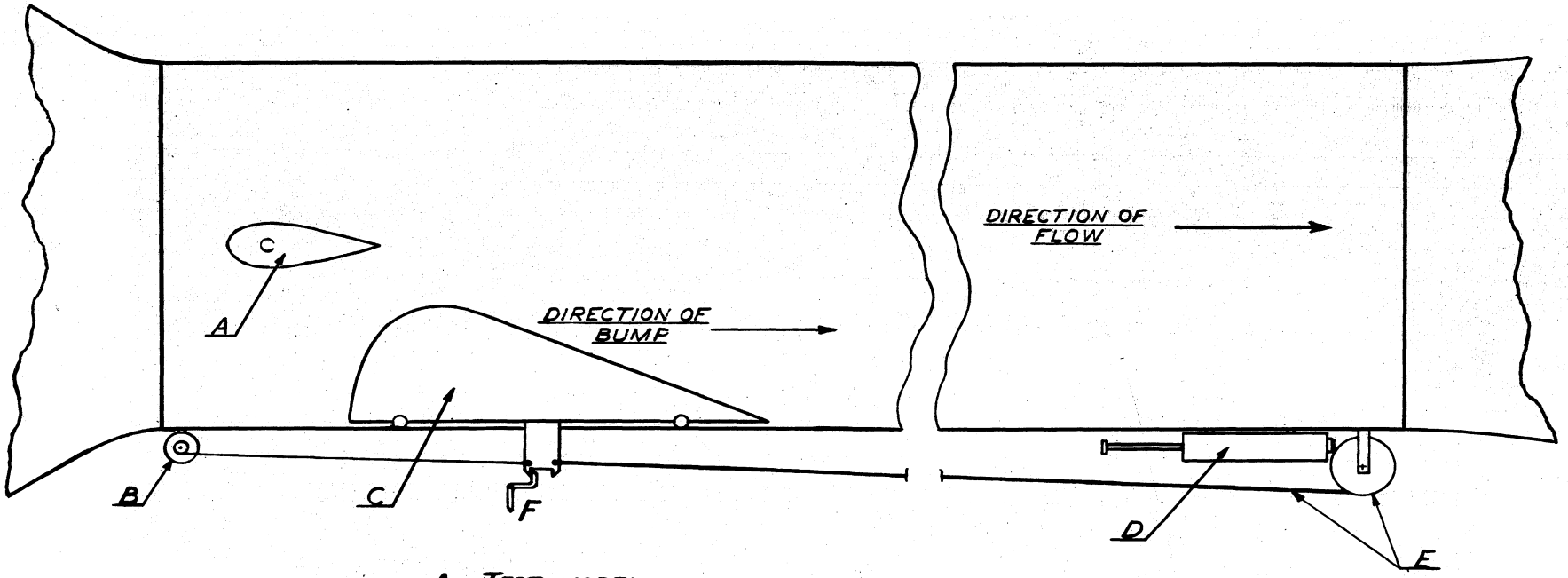

A. TEST MODEL.
B. POTENTIOMETER TO DETERMINE POSITION OF BUMP.
C. MOVING BUMP.
D. SHOCK ABSORBING CYLINDER.
E. ACCELERATING MECHANISM (AIRCRAFT SHOCK CORD & WINDING DRUM).
F. LATCH

Figure 6a. Schematic diagram of Moving Bump Gust Generator.

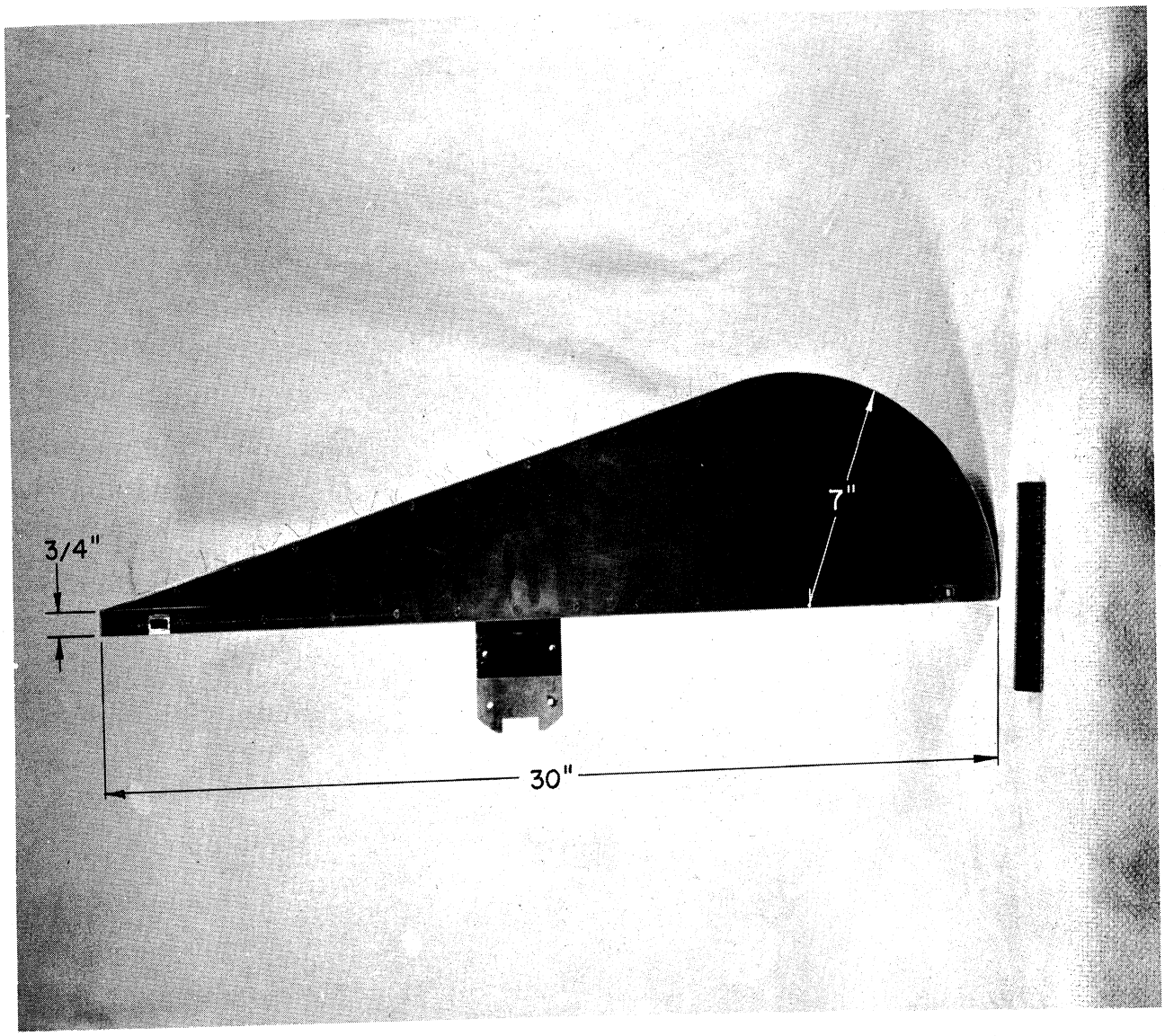

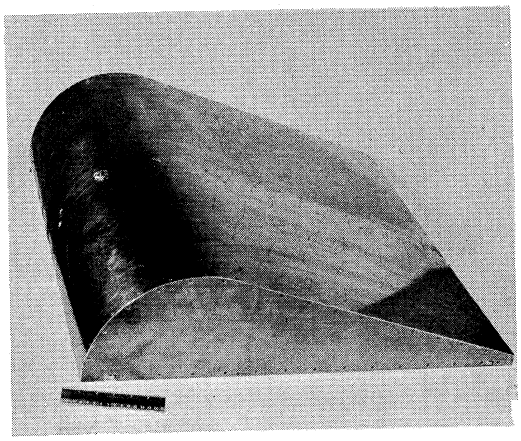

Figure 6b. Photographs of moving bump and its dimensions as used in 21-inch x 29-inch open-return tunnel.

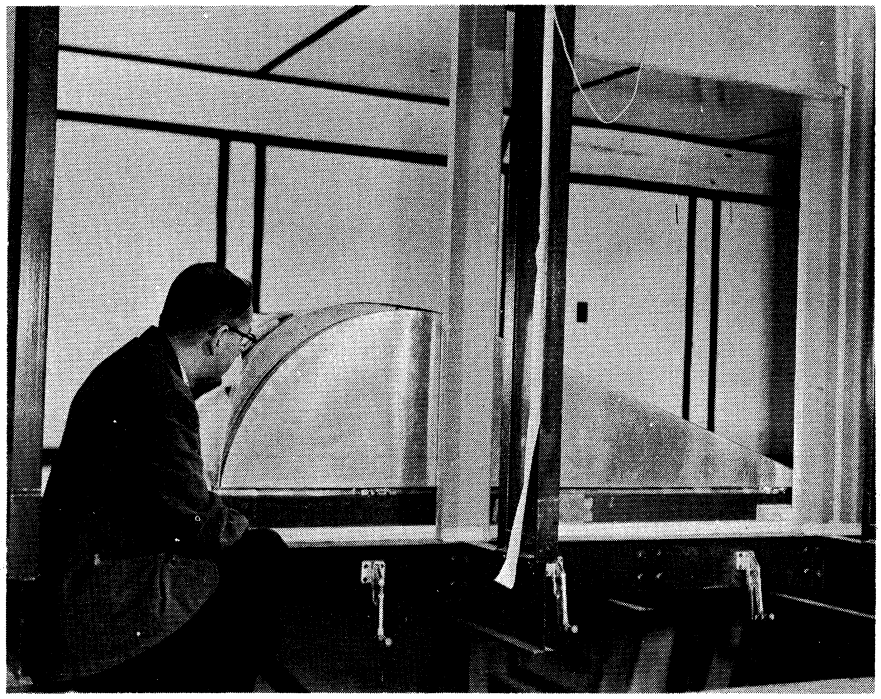

Figure 6c. Photograph of moving bump in 5-foot x 7-foot tunnel.

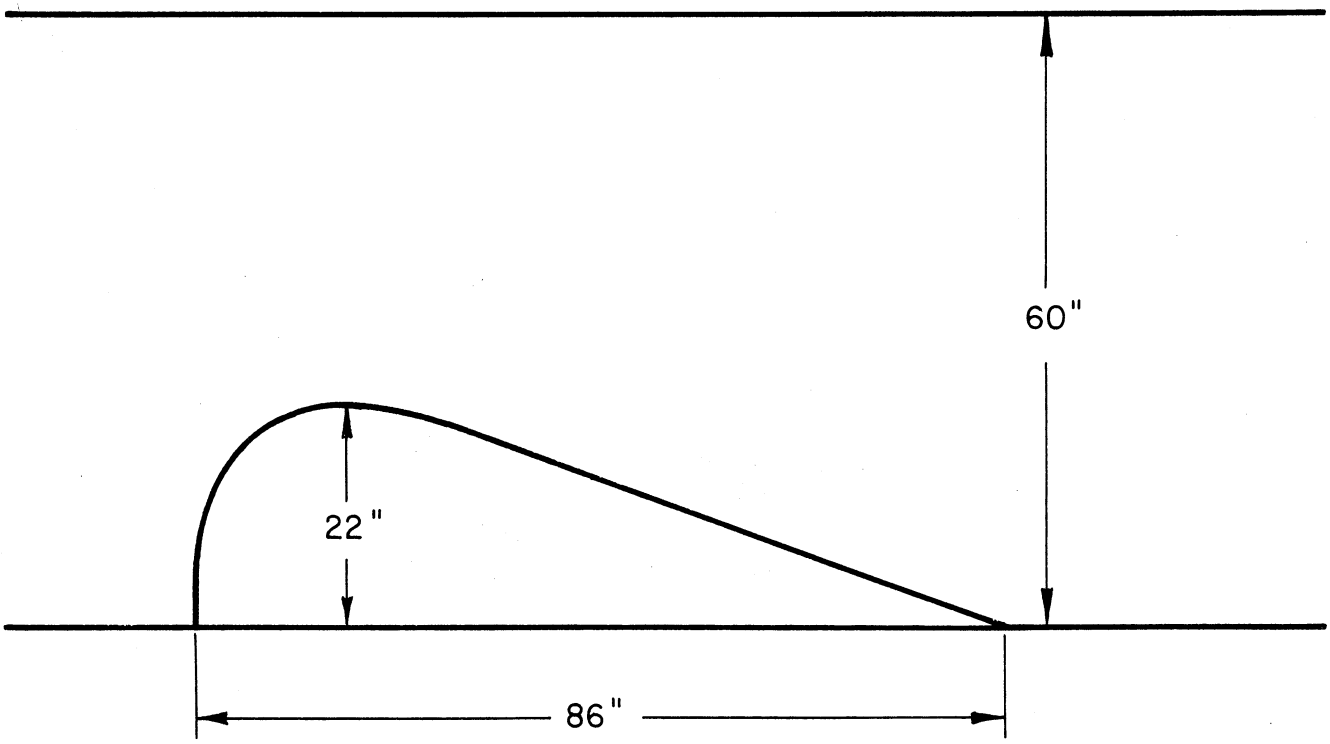

Figure 6d. Sketch of moving bump in 5-foot x 7-foot tunnel.

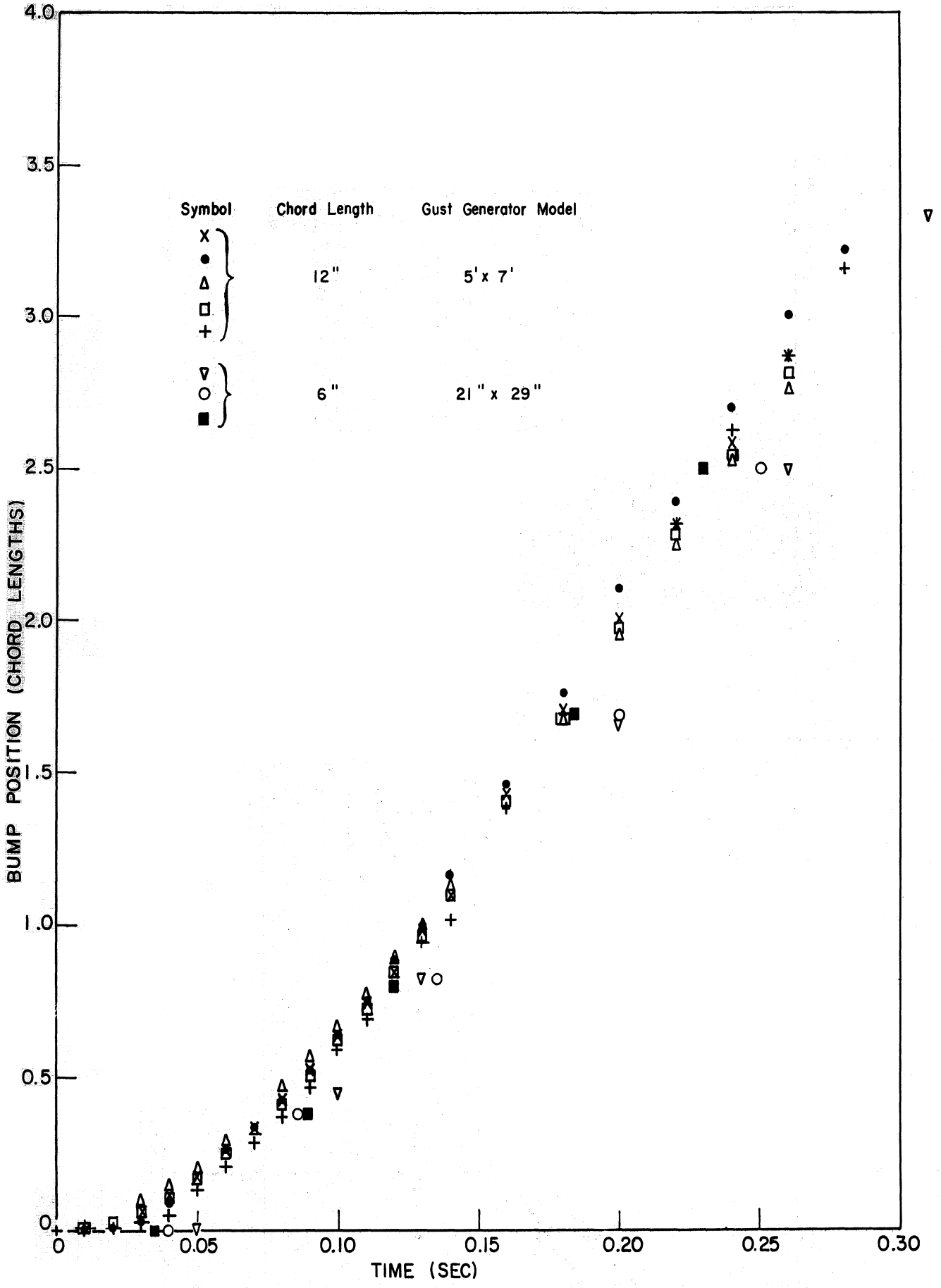

Figure 7. Bump position in chord lengths versus time.

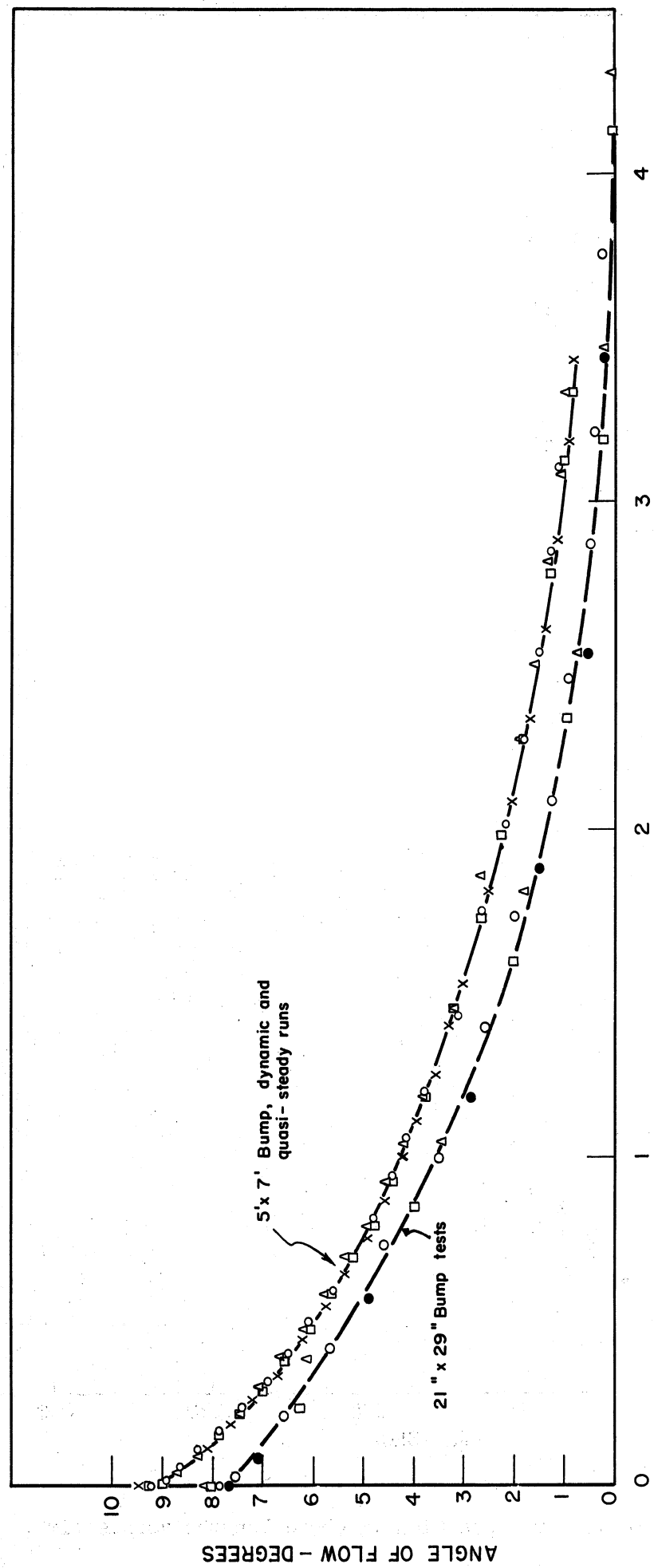

Figure 8. Flow inclination in degrees versus bump position in wing chords.

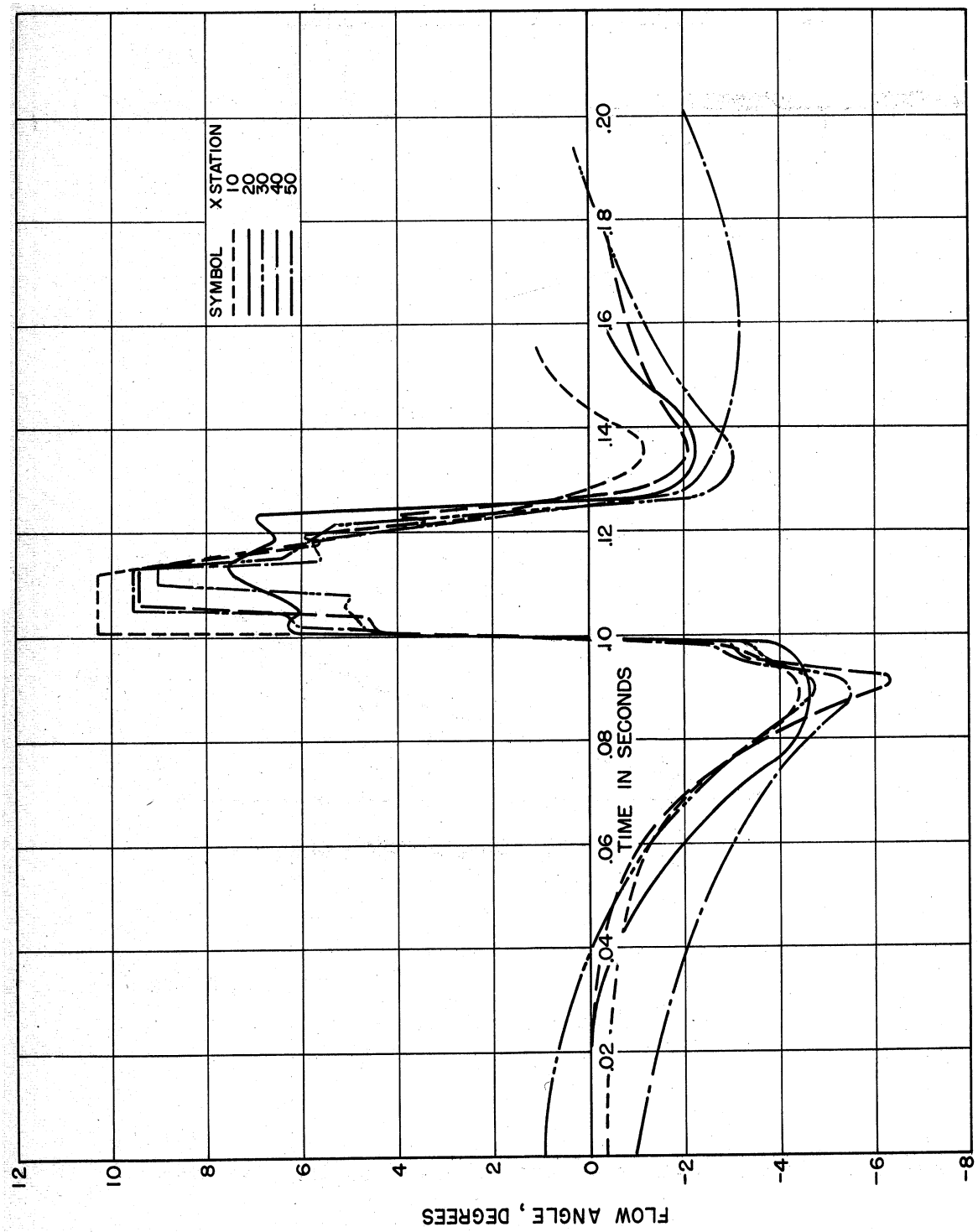

Figure 9. Flow deflection for Vortex Gust Generator versus time for various stations along tunnel axis.

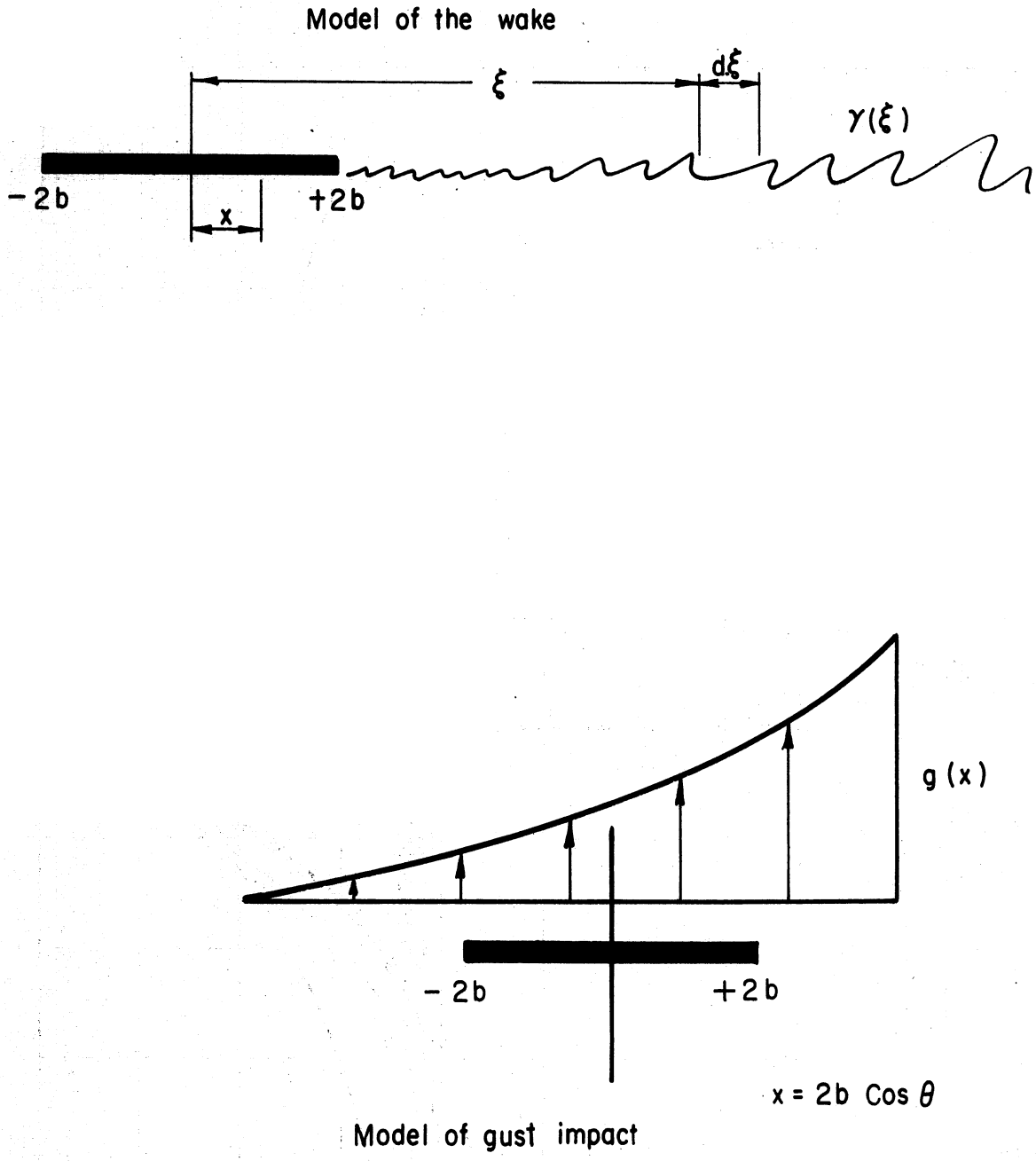

Figure 10. Sketch showing mathematical model of lift-lag system.

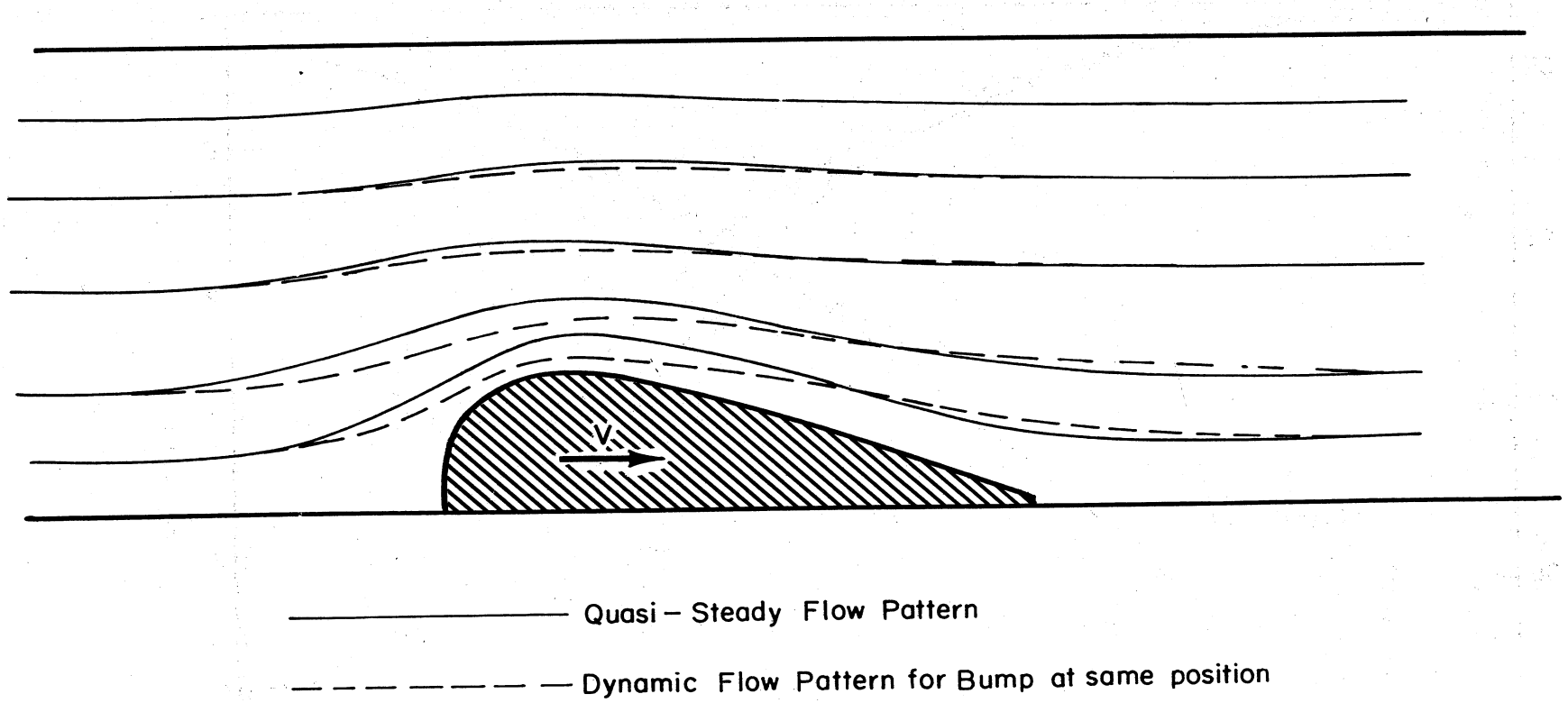

Figure 11. Quantitative effect of bump position upon flow-streamline distribution.

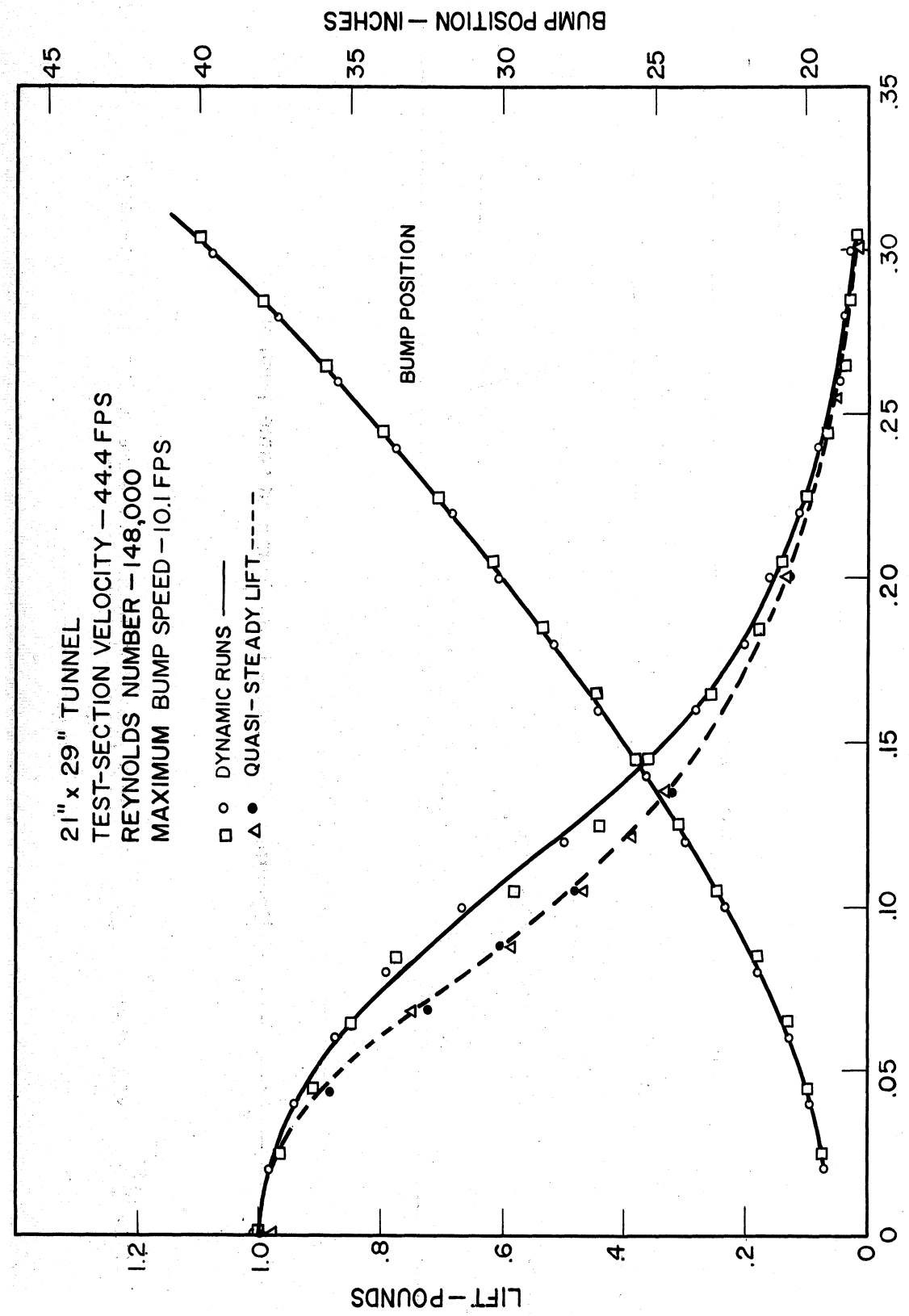

Figure 12. Measured dynamic lift, quasi-steady lift, and bump position versus time for a test-section velocity of 44.4 feet per second.

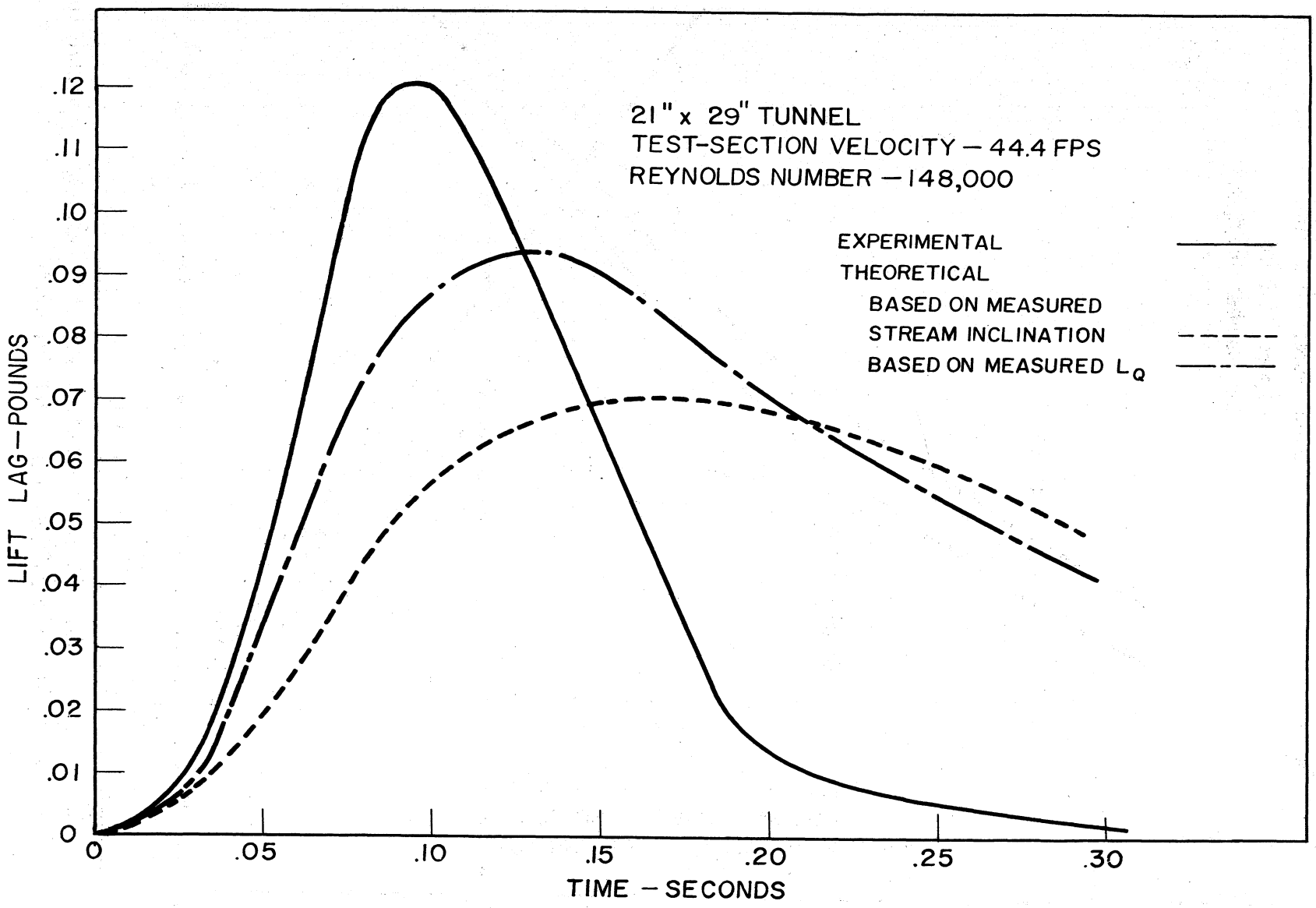

Figure 13. Comparison of experimental and theoretical lift lag versus time for test-section velocity of 44.4 feet per second.

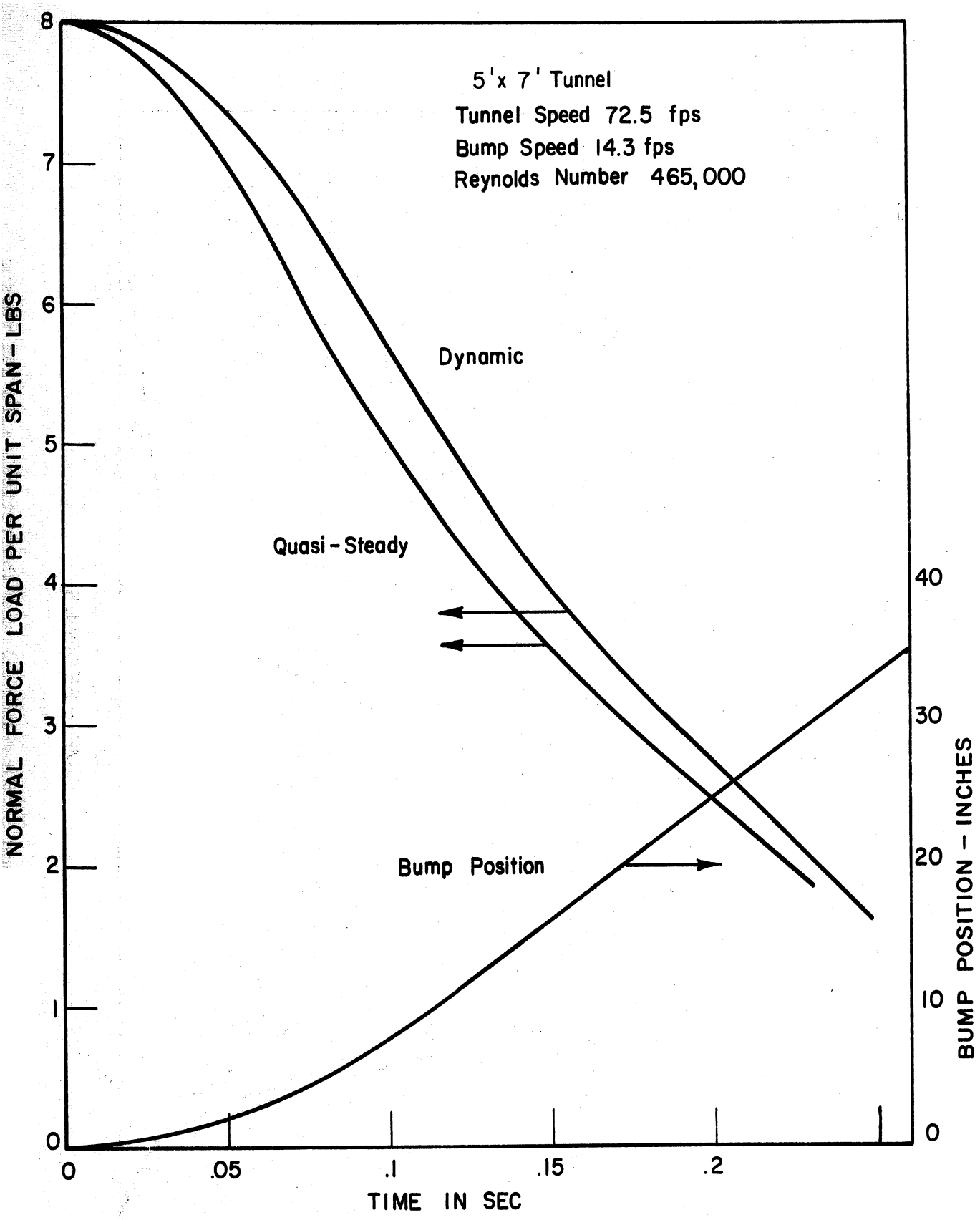

Figure 14. Measured dynamic lift, quasi-steady lift, and bump position versus time for test-section velocity of 72.5 feet per second.

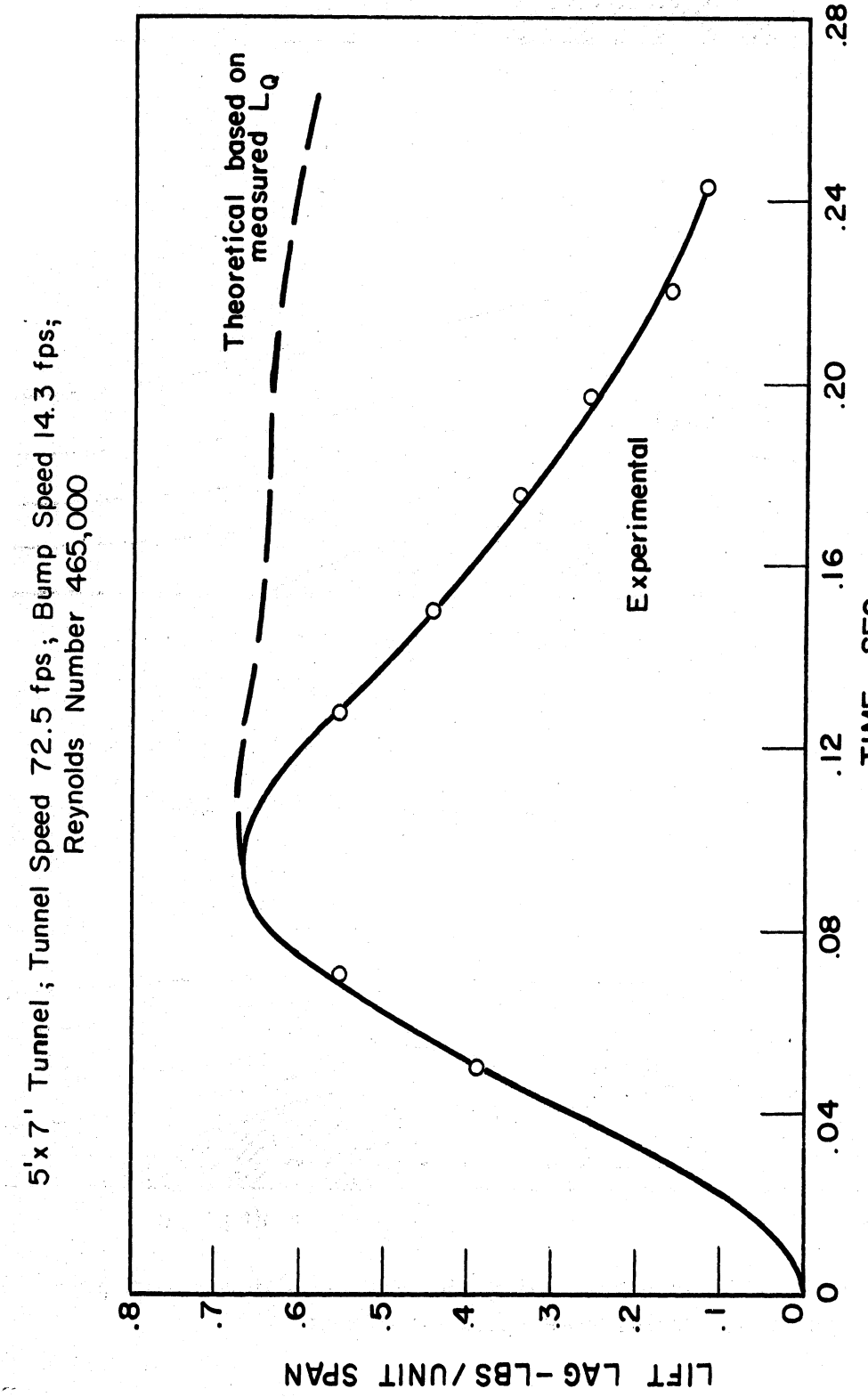

Figure 15. Comparison of theoretical and experimental lift lag for Moving Bump Gust Generator.

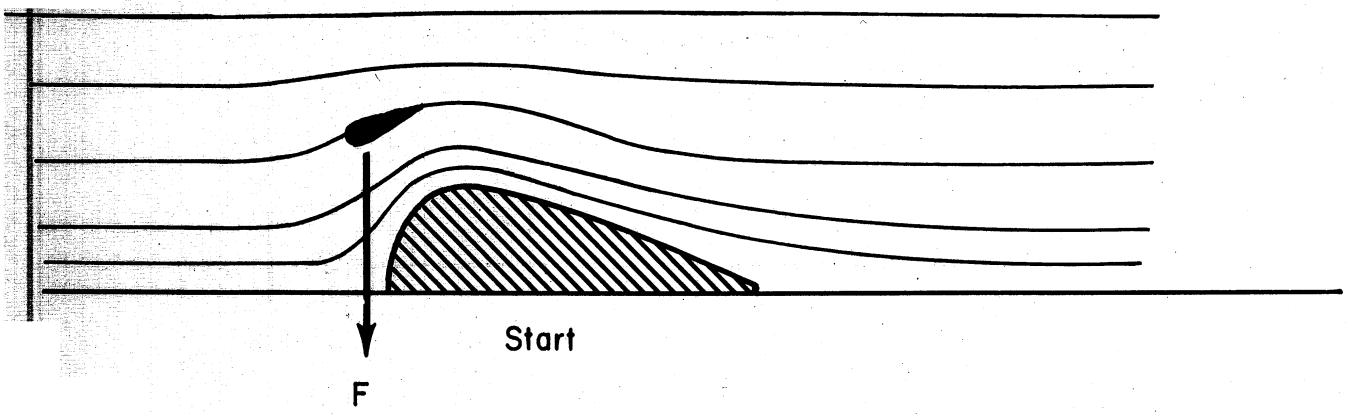

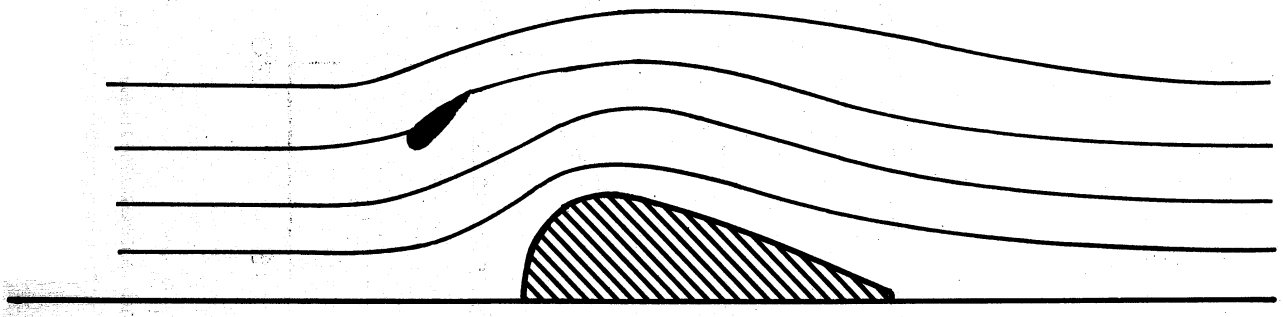

Bump in mid position

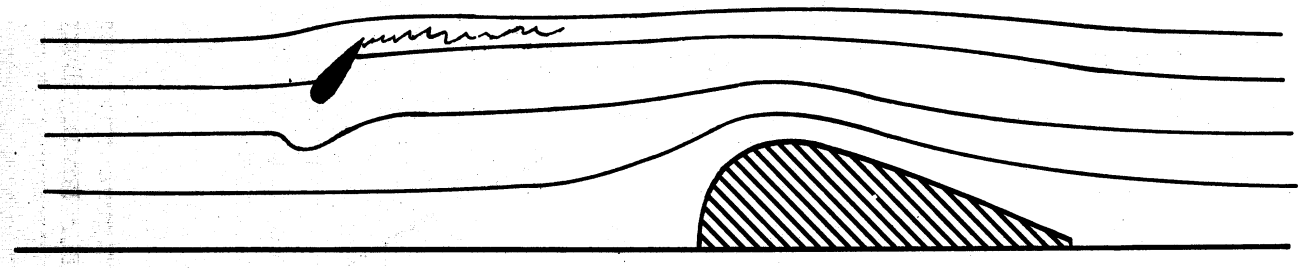

Bump in aft position

Figure 16. Sketch showing flow patterns at three bump positions for lift-overshoot experiment.

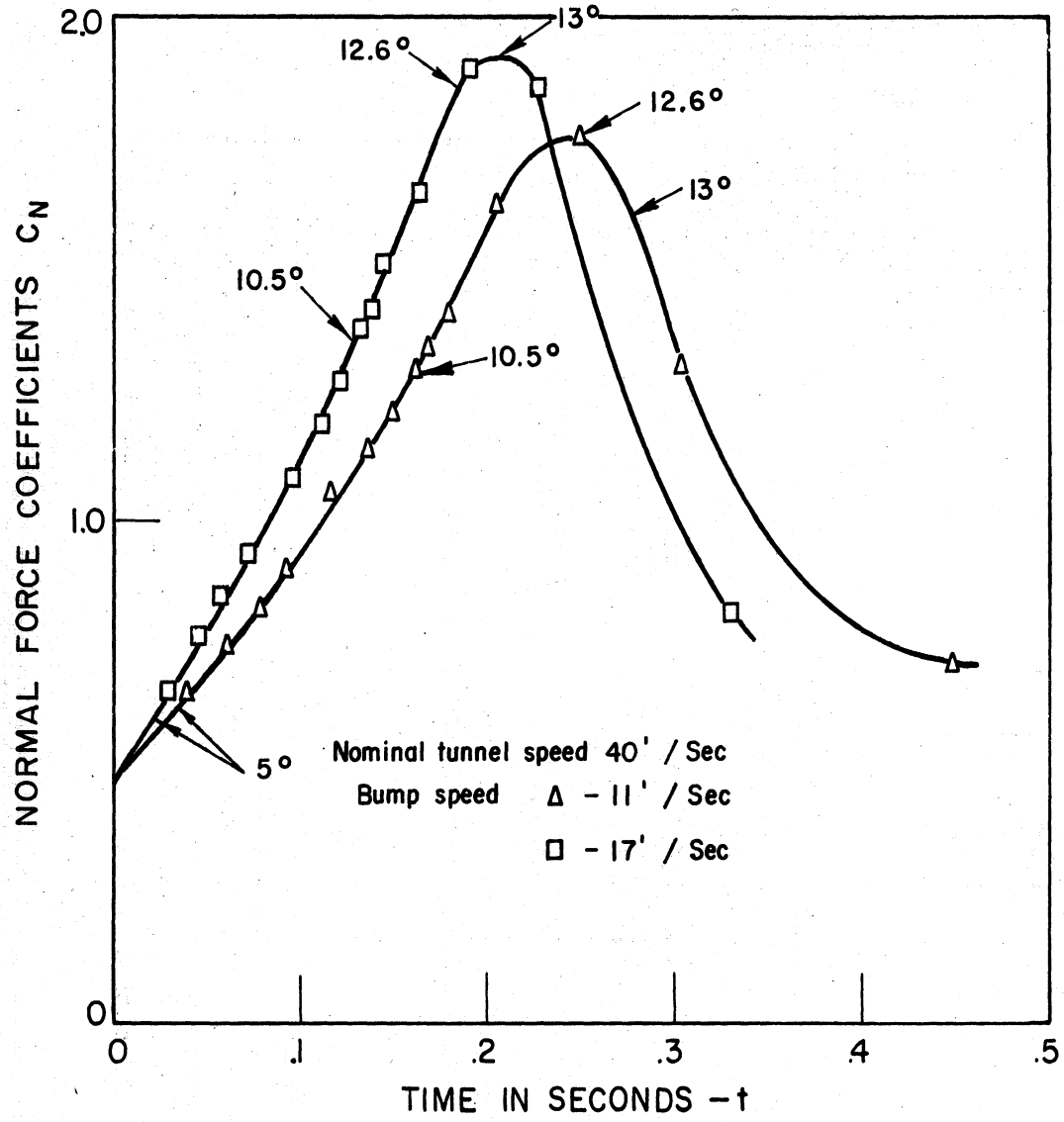

Figure 17. Lift response at two bump speeds in region of wing stall.

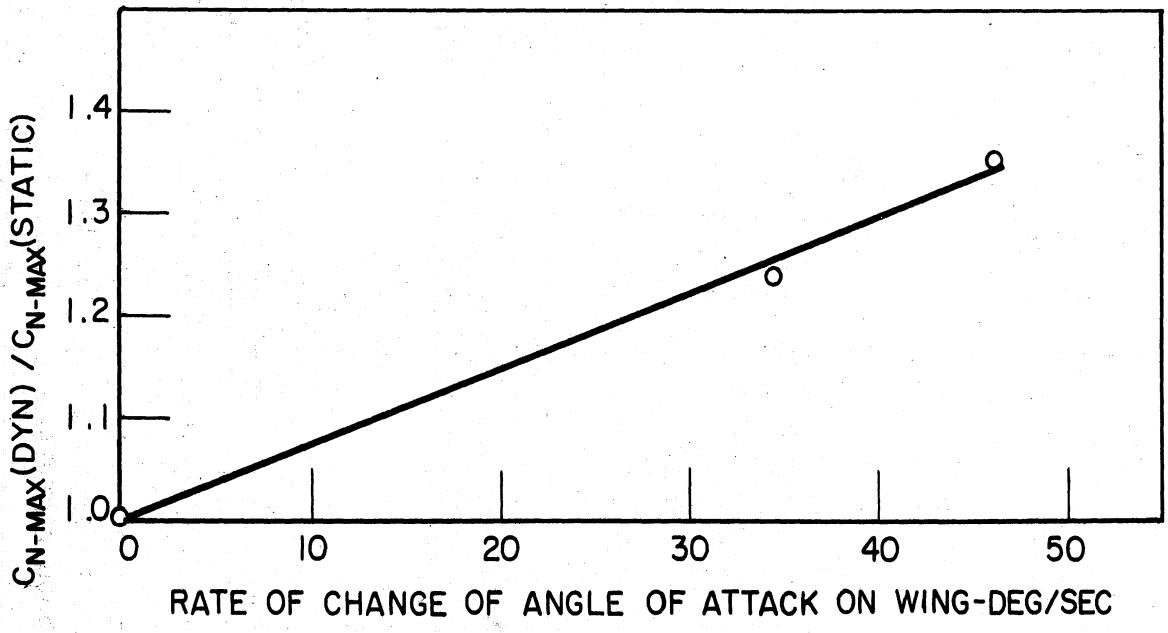

Figure 18. Effect of rate of change of angle of attack upon maximum normal force coefficient.

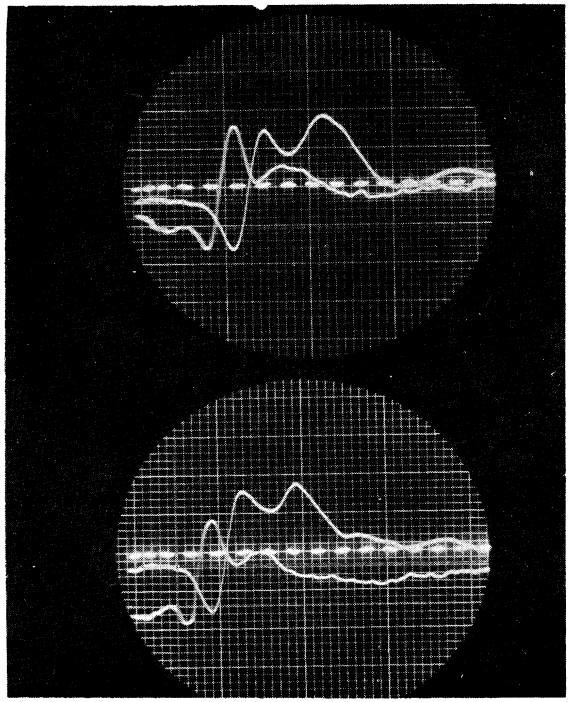

a

Tunnel speed = 59.7 ft/sec.
Dashed line is a 50-cps time pulse.
Monitor probe trace is first trace to cross time-pulse line in both pictures.
Lifting surface trace is second trace to cross time-pulse line in both pictures.

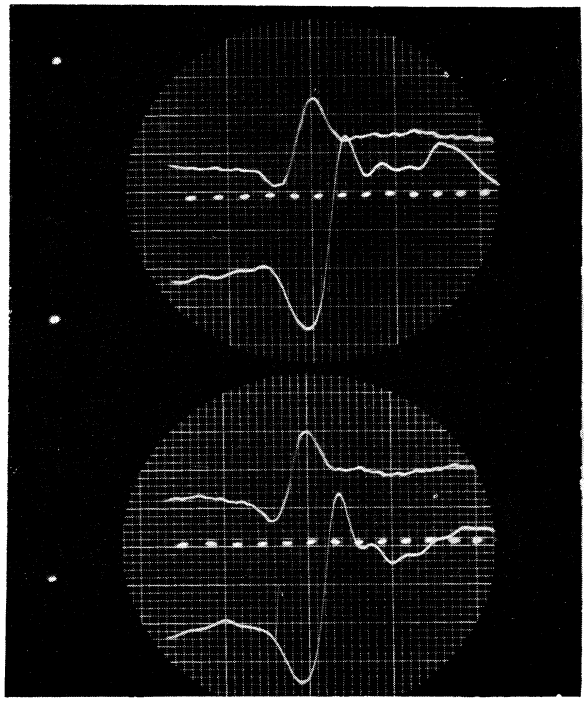

b

Tunnel speed = 30 ft/sec.
Dashed line is a 50-cps time pulse.
Monitor probe is upper trace in both pictures.
Lifting surface response is lower curve in both pictures.

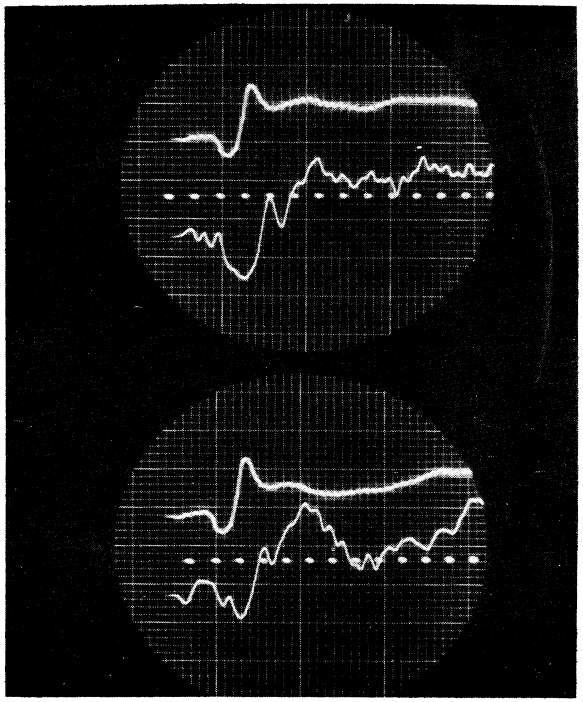

c

Tunnel speed = 15 ft/sec.
Dashed line is a 50-cps time pulse.
Monitor probe is upper curve in both pictures.
Lifting-surface response is lower curve in both pictures.

Figure 19. Oscillograms of the lifting-surface and monitor-probe responses to the Vortex Gust Generator.

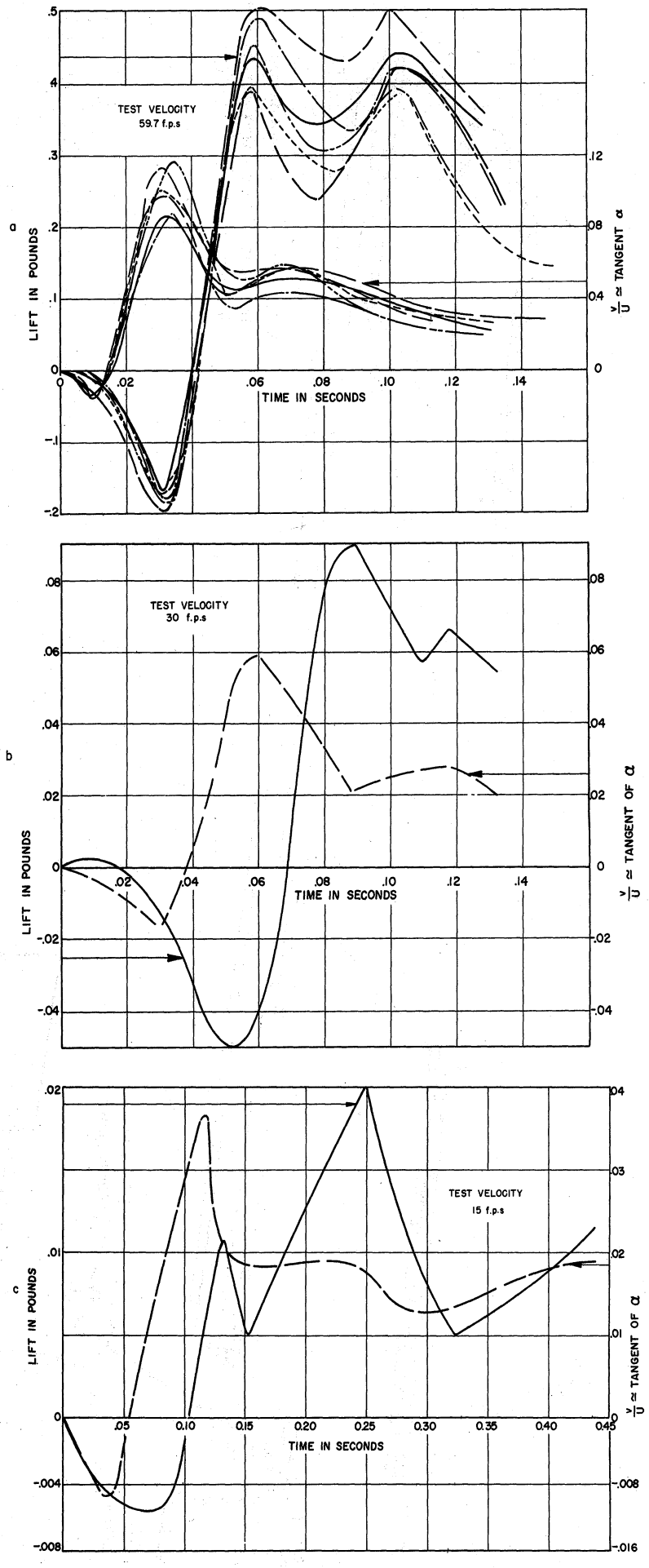

Figure 20. Responses of lifting-surface and hot-wire monitor probe to Vortex Gust Generator for three wind speeds.

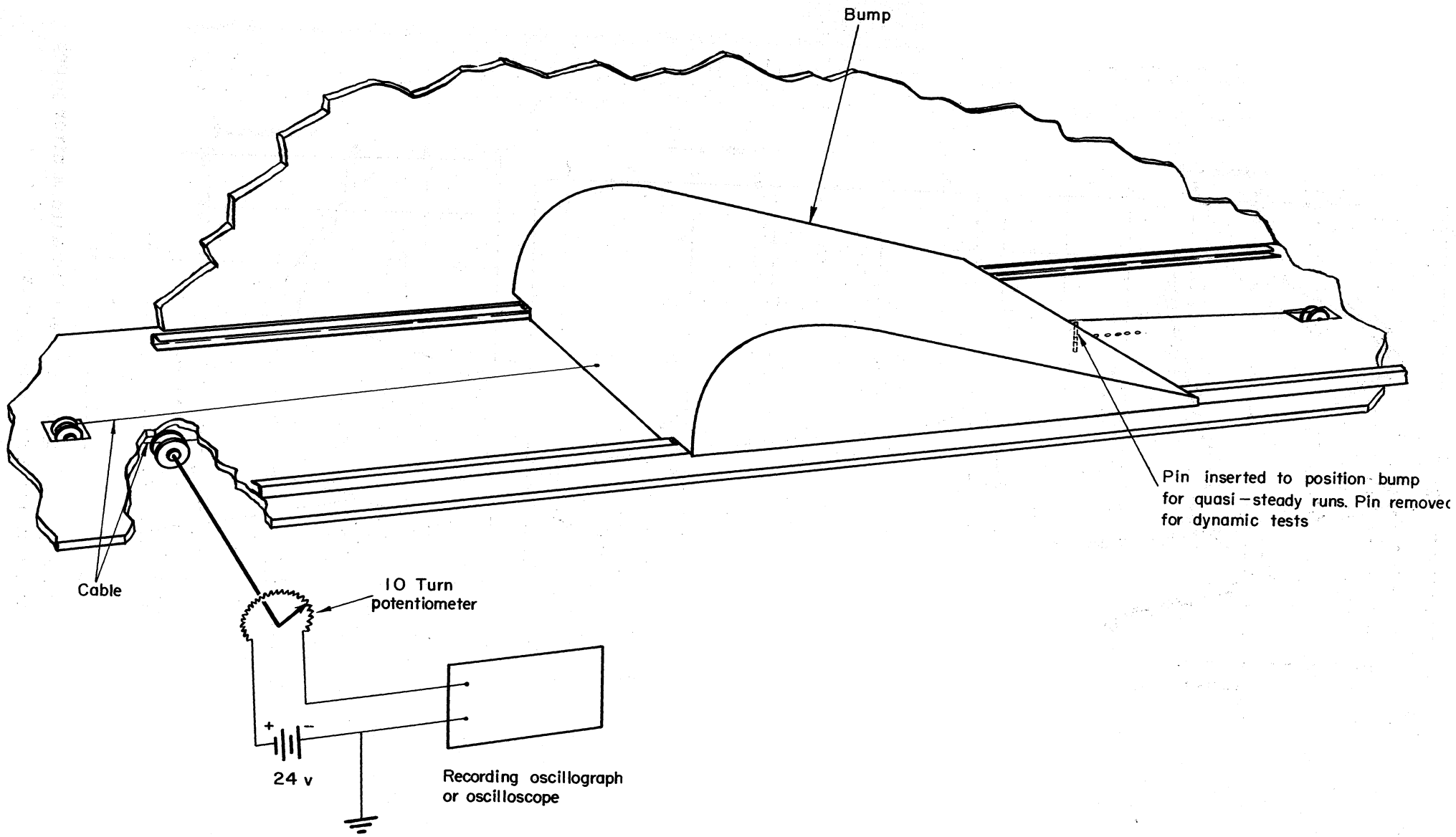

Figure 21. Sketch of bump-position mechanism.

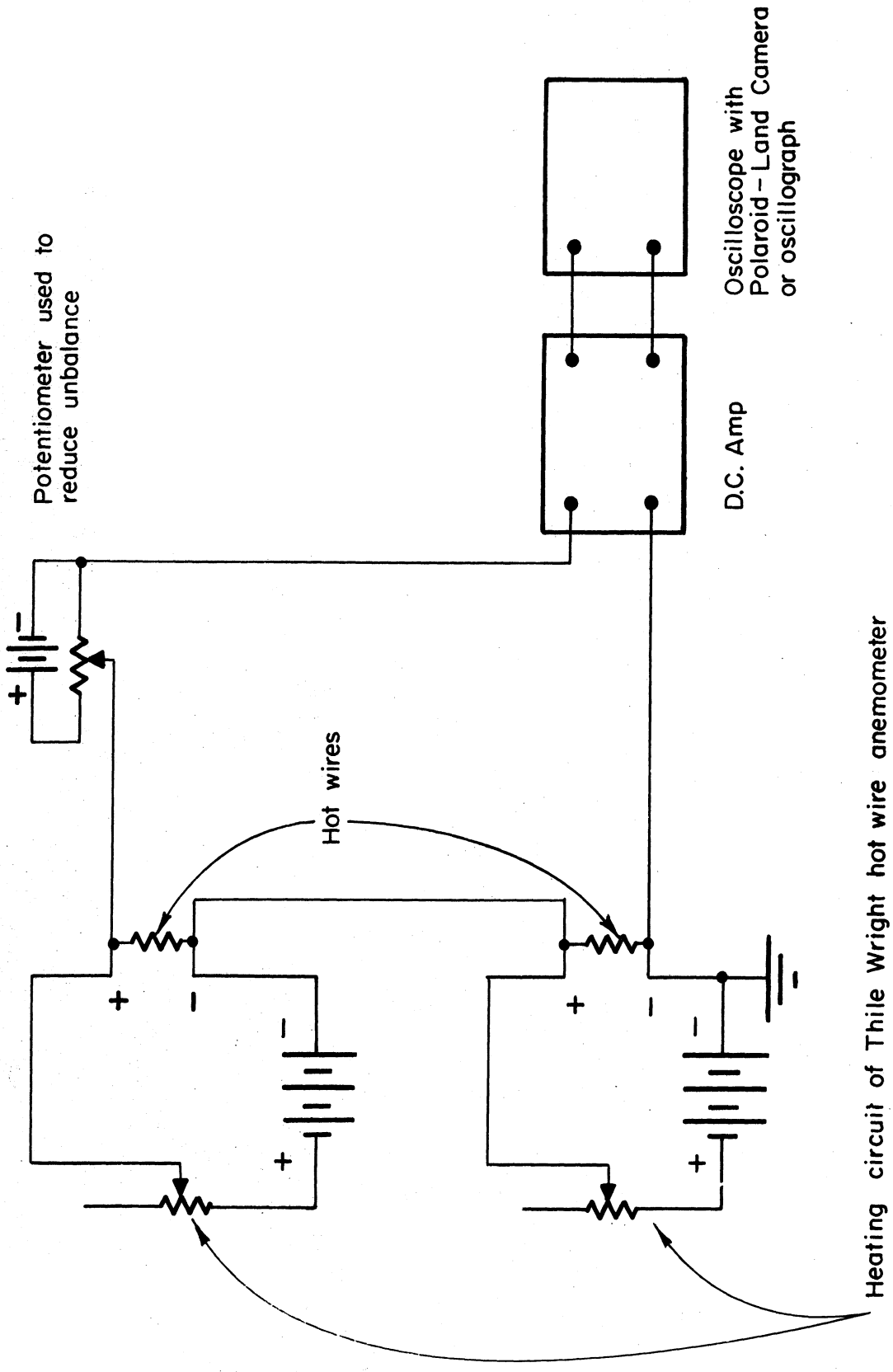

Figure 22. Electrical circuit used to measure flow angles.

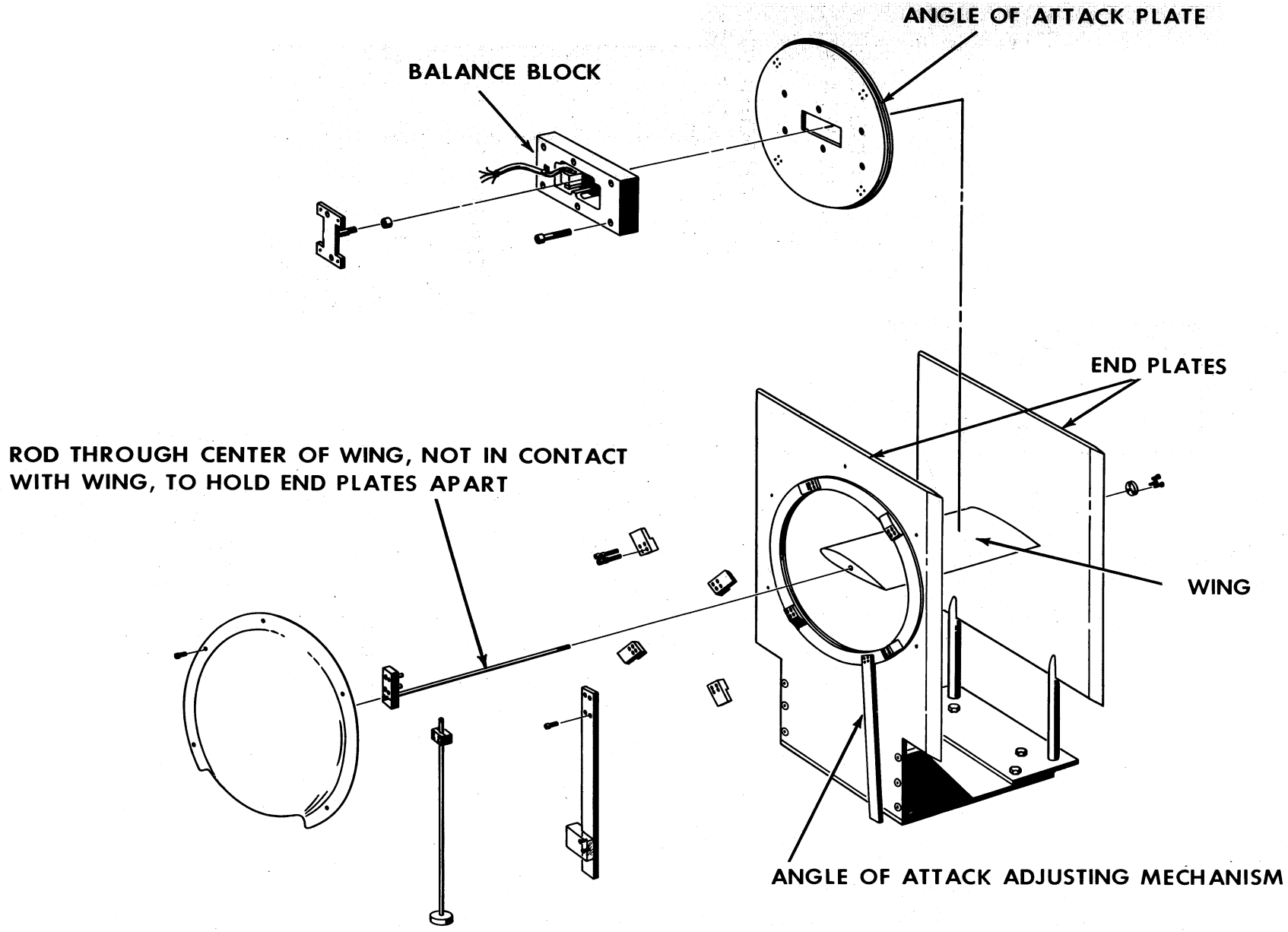

Figure 23a. Exploded view of balance as used in Moving Bump Gust Generator.

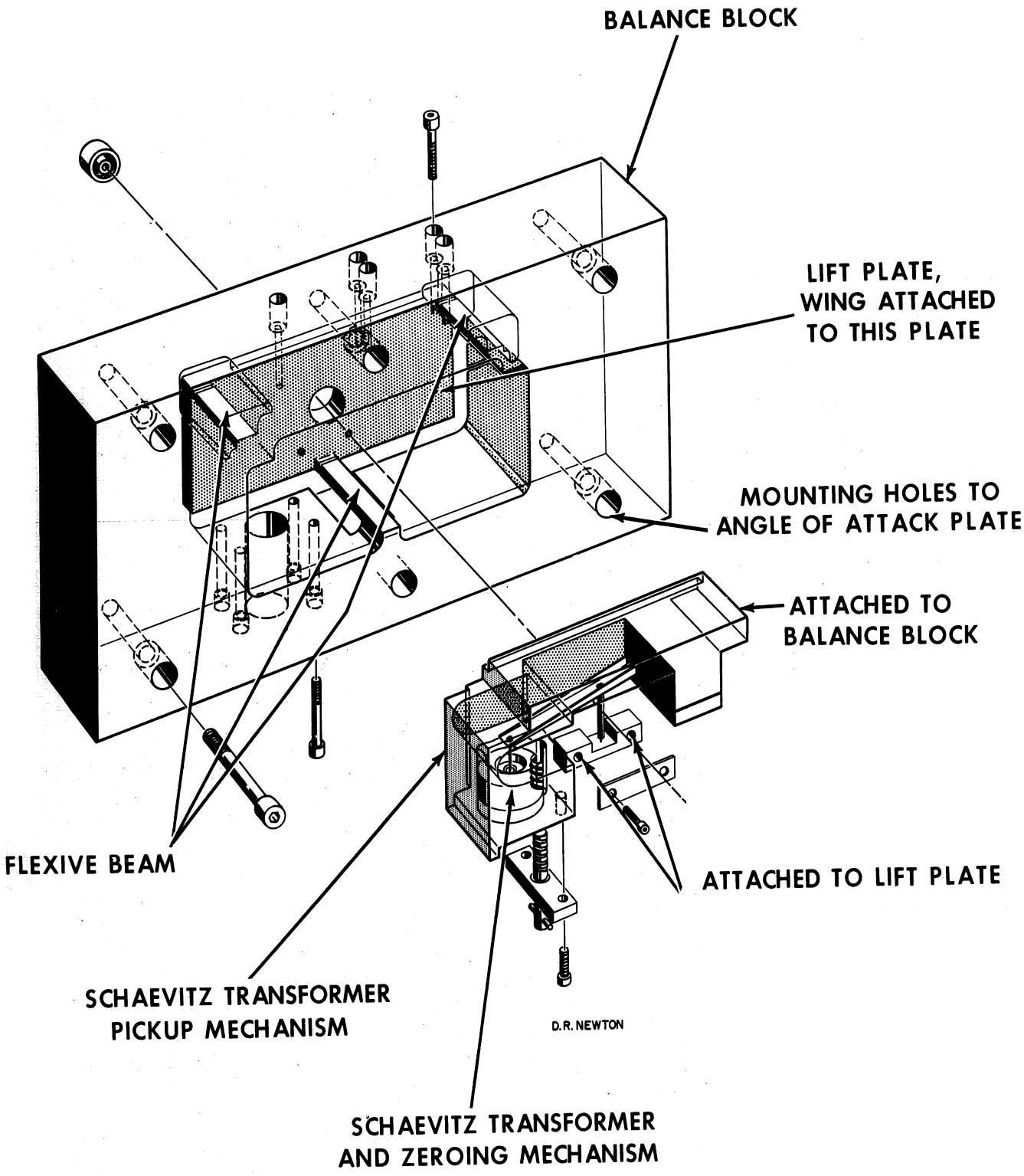

Figure 23b. View showing flexure-beam block and Schaevitz Transformer mounting.